



HAL
open science

Identification and Extraction of Surface Waves from Three-component Seismograms based on the Normalized Inner Product

Kristel Carolina Meza Fajardo, Apostolos Papageorgiou, Jean-François Semblat

► **To cite this version:**

Kristel Carolina Meza Fajardo, Apostolos Papageorgiou, Jean-François Semblat. Identification and Extraction of Surface Waves from Three-component Seismograms based on the Normalized Inner Product. Bulletin of the Seismological Society of America, 2015, 105 (1), pp.210-229. 10.1785/0120140012 . hal-02147535

HAL Id: hal-02147535

<https://hal.science/hal-02147535>

Submitted on 4 Jun 2019

HAL is a multi-disciplinary open access archive for the deposit and dissemination of scientific research documents, whether they are published or not. The documents may come from teaching and research institutions in France or abroad, or from public or private research centers.

L'archive ouverte pluridisciplinaire **HAL**, est destinée au dépôt et à la diffusion de documents scientifiques de niveau recherche, publiés ou non, émanant des établissements d'enseignement et de recherche français ou étrangers, des laboratoires publics ou privés.

1 TITLE:

2 **Identification and Extraction of Surface Waves from Three-component Seismograms based on the**
3 **Normalized Inner Product**

4

5 AUTHORS' NAMES:

6 Kristel C. Meza-Fajardo⁽¹⁾, Apostolos S. Papageorgiou⁽²⁾ and Jean-François Semblat⁽³⁾

7

8 CORRESPONDING AUTHOR:

9 Kristel C. Meza-Fajardo

10 Department of Civil Engineering,

11 Universidad Nacional Autónoma de Honduras

12 Tegucigalpa, Honduras

13 E-mail: kristelmeza@unah.edu.hn

14

15

16 **ABSTRACT**

17 Identification of different wave types in a seismogram is an important step for the understanding of
18 wave propagation phenomena. Since in most seismograms, different types of waves with different
19 frequencies may appear simultaneously, separation of waves is more effectively achieved when a time-
20 frequency analysis is performed. In this work, we propose a new time-frequency analysis procedure to
21 identify and extract Rayleigh and Love waves from three-component seismograms. Exploiting the
22 advantage of the absolute phase preservation by the Stockwell Transform, we construct time-frequency
23 filters to extract waves based on the ‘Normalized Inner Product’ (NIP). Since the NIP is the time-
24 frequency counterpart of the correlation, Rayleigh and Love waves can be identified depending on the
25 NIP between the Stockwell Transforms of the horizontal and vertical displacement components. The
26 novelty and advantage of the proposed procedure is that it does not require specifying a-priori the
27 direction of propagation of the surface waves, but instead such direction is determined. Furthermore, it is
28 shown that the NIP is a more stable parameter in the time-frequency domain when compared to the
29 instantaneous reciprocal ellipticity, and thus it avoids smoothing (and with it, altering) the data. The
30 procedure has been successfully tested with real signals, specifically to extract Rayleigh and Love waves
31 from seismograms of one aftershock of the 1999 Chi-Chi earthquake. With the proposed procedure we
32 found different directions of propagation for retro-grade and pro-grade Rayleigh waves, which might
33 suggest that they are generated by different mechanisms.

34 INTRODUCTION

35 The identification of surface waves in a time history is one of the fundamental tasks in seismology.
36 Surface waves are important not only because they carry information about the surficial geological
37 layers in which they propagate, but also for their impact on man-made structures. Methods for
38 identifying surface waves are based on the two main characteristics of such waves: (1) plane and type of
39 polarization, and (2) frequency-dependent phase velocities (dispersion). A processor to identify surface
40 waves and simultaneously compute their azimuth, was proposed in the late 70's by Smart (1978). The
41 algorithm finds the best fit between polarization characteristics of ground motion and surface wave
42 models defined in the frequency domain. More recently, identification of Rayleigh wave phases has
43 been performed by means of Complex Trace Analysis (CTA) (Vidale, 1986, René *et al.*, 1986, Li and
44 Crampin, 1991, Baker and Stevens, 2004). CTA uses time-varying polarization characteristics to
45 differentiate between waves, and thus, waves arriving at different times can be separated. Rayleigh
46 waves are identified by considering the fact that they are elliptically polarized in a plane oriented in their
47 direction of propagation. However, in view of the fact that dispersed waves (such as surface waves) may
48 be effectively described and analyzed in terms of narrow-band wave packets, we need an extraction
49 technique that resolves the recorded signals in such narrow-band packets. Since CTA does not provide
50 information on the time variation of the frequency content of the signal, the analyst needs to choose
51 frequency ranges of interest *a priori*. This problem is aggravated when different types of waves appear
52 simultaneously in the signal under investigation, as it often happens with seismic waves. Another
53 difficulty faced by the analyst is the need to assume *a priori* the direction of propagation of the surface
54 waves present in the time histories.

55 Considering the above reasons, a time-frequency polarization analysis seems to be a more appropriate
56 alternative in order to separate the different phases in a wave field. Whereas most of classical signal
57 processing studies of the 1970s were aimed at stationary signals and processes, many efforts were
58 devoted to less idealized situations during the 1980s, and the idea of time-frequency analysis
59 progressively emerged as a new paradigm for non-stationarity. It is now well recognized that many
60 signal processing problems can be advantageously phrased in a time-frequency language. Pinnegar
61 (2006) and Galiana-Merino *et al.* (2011) have constructed filters to exclude or extract Rayleigh waves
62 using their elliptical polarization as filtering criterion. However, filtering based on the elliptical
63 polarization attribute alone does not work well if the time history contains Rayleigh waves with both
64 retro-grade and pro-grade motion. Such a case has been observed in recordings of the aftershock 1803 of
65 the Chi-Chi earthquake that occurred on 20 September 1999 with magnitude Mw 6.2 (Wang *et al.*,
66 2006). The method we propose herein to detect and extract surface waves from three-component
67 recorded seismograms overcomes these difficulties. We exploit the advantage of the absolute phase
68 preservation of the Stockwell Transform (Stockwell *et al.*, 1996), and we construct time-frequency
69 filters to extract waves based on the ‘Normalized Inner Product’ (NIP). Since the NIP is the time-
70 frequency counterpart of the correlation, Rayleigh and Love waves can be identified based on the value
71 of the NIP between the Stockwell Transforms of the horizontal and vertical displacement components.
72 The proposed procedure does not require specifying a-priori the direction of propagation of the surface
73 waves, but instead such direction is determined with the proposed computational procedure.

74 **TIME-FREQUENCY POLARIZATION ANALYSIS**

75 Polarization characteristics are useful tools to identify and separate different types of waves present in a
76 multi-component signal. If the components of the analyzed signal are in-phase, it is said that they are

77 linearly polarized. When the components are 90 degrees out-of-phase and have the same amplitude, the
78 state corresponds to circular polarization. If the components are 90 degrees out-of-phase and have
79 different amplitudes, the state corresponds to elliptical polarization. Regarding waves contained in
80 seismic signals, the polarization state observed for Rayleigh waves is elliptical (either retro-grade or pro-
81 grade), whereas body and Love waves are considered to be linearly polarized.

82 Following the ideas presented by Pinnegar (2006), three-component signals can be thought as a
83 superposition of sinusoids oscillating along the x , y , and z axes, which when considered one
84 frequency at a time, trace out elliptical motion in 3D space. Thus, the total three component signal can
85 be thought of as a superposition of ellipses, which are characterized by descriptive parameters such as
86 the length of the semi-minor and semi-major axis, the strike and dip of each ellipse plane, the pitch of
87 the major axis, and the phase of the particle motion at each frequency. The Fourier spectra of the
88 descriptive parameters of the superimposed ellipses can be related to the Fourier transforms of the x , y
89 and z components (Pinnegar, 2006). The same type of reasoning can be used with windowed Fourier
90 transforms (such as the Stockwell Transform), so as to provide time-varying spectra for the
91 abovementioned descriptive parameters. Details on how the attributes of the ellipses are defined for
92 three-component signals can be found in Pinnegar (2006).

93 In this work, we adopt the Stockwell Transform for the mapping between time and time-frequency
94 domains, because: 1) using the Stockwell Transform, we retain the absolute phase of each localized
95 frequency component (Stockwell *et al.*, 1996), and 2) the invertibility of the Stockwell Transform allows
96 for the wave extraction by simple filtering in the time-frequency domain. The Stockwell Transform is a
97 generalization of the short-time Fourier transform (STFT), and may be thought of as an extension of the
98 continuous wavelet transform (CWT) while overcoming some of its disadvantages. It is based on a

99 moving and scalable localizing Gaussian window, which features a standard deviation that is always
 100 equal to one wavelength of the Fourier sinusoid (Pinnegar, 2006). The “moving window” technique has
 101 been already used in the past in surface wave analyses (Flinn, 1965; Dziewonski *et al.*, 1969; Vidale,
 102 1986) based on the concept of the “analytical signal” of the time series. It can be shown (Stockwell,
 103 2007) that the Stockwell Transform at a specific frequency is closely related to the analytical signal of
 104 the time series, when the time series is bandpass filtered using the Gaussian window. The Stockwell
 105 transform of a time varying function can be expressed in the following form (Stockwell *et*
 106 *al.*, 1996):

$$\text{---} \quad \text{---} \quad (1)$$

107 where is the center of the Gaussian window. The time-frequency parameters of the polarization ellipse,
 108 which describe the contribution of the -th frequency to the total signal are defined in Pinnegar (2006)
 109 in terms of the Stockwell transform. In particular, Pinnegar (2006) and Galiana-Merino *et al.* (2011)
 110 have used the ratio of the semi-minor to the semi-major axis of the polarization ellipse to identify
 111 Rayleigh waves contained in a seismic signal. This ratio is called in Galiana-Merino *et al.* (2011)
 112 “instantaneous reciprocal ellipticity” (IRE), and is defined as:

$$\text{---} \quad (2)$$

113 where and are the semi-major and semi-minor axis of the ellipse, respectively. For a
 114 three-component signal these axes are given by the following expressions (Pinnegar 2006):

$$\begin{aligned} & \frac{\Re\{S_x(t, \omega)\}}{\Im\{S_x(t, \omega)\}} = \frac{\Re\{S_y(t, \omega)\}}{\Im\{S_y(t, \omega)\}} \\ & \frac{\Re\{S_z(t, \omega)\}}{\Im\{S_z(t, \omega)\}} = \frac{\Re\{S_w(t, \omega)\}}{\Im\{S_w(t, \omega)\}} \end{aligned} \quad (3)$$

115 where

$$(4)$$

116 Here $\Re\{S_x(t, \omega)\}$ and $\Im\{S_x(t, \omega)\}$ are the real and imaginary parts of the Stockwell transform of the x -component of the
 117 signal (we omit the arguments t and ω to avoid clutter). Similarly, $\Re\{S_y(t, \omega)\}$ and $\Im\{S_y(t, \omega)\}$ are pairs of the real
 118 and imaginary parts of the Stockwell transform for the y - and z -components of the signal, respectively.
 119 Note that the major axis a of the polarization ellipse is composed of two parts, a_{linear} and a_{circular} . Since the
 120 semi-minor axis b corresponds to the radius of the circular polarization, the segment a_{linear} will be the
 121 part corresponding to linear polarization. Therefore, if the polarization state is circular, $a_{\text{linear}} = 0$, and
 122 consequently $a = b$. If the polarization is linear, $b = 0$, and then $a = a_{\text{linear}}$. The IRE can then be
 123 used to discern the different waves contained in a seismic signal. To identify Rayleigh waves, Galiana-
 124 Merino *et al.* (2011) and Pinnegar (2006) have considered values of a/b greater than 1. Using this
 125 criterion, filters to extract the desired wave from the signal can be readily constructed. The filters are
 126 applied in the time-frequency domain (t, ω) , and then the Inverse Stockwell Transform is used to
 127 recover the filtered time-domain signal. The Inverse Stockwell Transform is computed in two steps:

128 first, the Fourier Transform of the original signal is obtained by integrating the Stockwell transform over
129 time , and then the Fourier Transform is inverted (Stockwell *et al.*, 1996).

130 Galiana-Merino *et al.* (2011) made use of the IRE to extract Rayleigh waves adopting the Stationary
131 Wavelet Packet Domain (SWPD) method. However their approach requires knowledge, in advance, of
132 the direction of propagation of the Rayleigh waves in order to be applied. In Galiana-Merino *et al.*
133 (2011) it is suggested that this direction will be the “radial” direction of wave propagation (i.e. the back-
134 azimuth to the epicenter). However this assumption may not be correct if the waves are generated by
135 diffraction at the edge of a basin, or if they are waves trapped inside the basin. Thus, in Galiana-Merino
136 *et al.* (2011) the horizontal components are rotated to obtain the radial component and then, the vertical
137 and radial components are used to compute the IRE. On the contrary, the IRE, defined by Pinnegar
138 (2006) as in Eq. (2), is computed using the three components of the signal and it does not change when
139 the horizontal components are rotated. However, even after extracting the waves (i.e. their components
140 along two arbitrary orthogonal axes), their direction of propagation is not provided by the filtering
141 process using the value of the IRE as the criterion.

142 **DIRECTION OF SURFACE WAVE POLARIZATION**

143 Once the polarization filtering has been completed, the angle of propagation of the extracted Rayleigh
144 waves may be estimated by correlating the filtered signals. One way to accomplish this is to use the
145 Chael-Selby-Baker-Stevens technique of calculating the back-azimuth of Rayleigh waves (Chael, 1997;
146 Selby, 2001; Baker and Stevens, 2004). The basic idea of this approach is to find an azimuth for which
147 the vertical and Hilbert-transformed radial component particle motions form a straight line (i.e. they are
148 linearly polarized). First, the two horizontal components are rotated into assumed radial and transverse
149 directions, with a trial back-azimuth ranging from to . The computed radial component is then

150 shifted in time using the Hilbert Transform. The shift must be a phase delay for pro-grade motion or
 151 phase advance for retro-grade motion (see Figure 1). The last step is the computation of the cross
 152 correlation between the vertical and Hilbert-transformed horizontal (radial) traces with the following
 153 formula:

$$\text{Correlation} = \frac{\int u(t) \tilde{v}(t) dt}{\sqrt{\int u^2(t) dt \int \tilde{v}^2(t) dt}} \quad (5)$$

154 where

$$\tilde{v}(t) = \int_{-\infty}^{\infty} \hat{v}(\omega) e^{-i\pi/2 \text{sgn}(\omega)} e^{i\omega t} d\omega \quad \text{or} \quad (6)$$

155 the function $u(t)$ is the vertical displacement component and $v(t)$ is the Hilbert-transformed radial
 156 displacement component. The estimated direction of the Rayleigh wave propagation corresponds to the
 157 direction (θ) that provides the maximum correlation, as θ sweeps the range 0 to π .

158 Clearly, the Chael-Selby-Baker-Stevens technique is a procedure that relies on sweeping the entire
 159 parameter space and selecting the value that returns the highest correlation. Here we propose a more
 160 direct procedure to compute the direction of propagation of the surface waves. Let us assume that the
 161 recorded motion consists of three components: $u(t)$ along the N-S direction (positive pointing to the
 162 North); $v(t)$ along E-W direction (positive pointing to the East); and $w(t)$ in the vertical direction
 163 (positive pointing up). Then, if the above-defined horizontal components were rotated by an angle
 164 (positive clockwise, as shown in Figure 2), so as to render: the radial component $r(t)$ (along the
 165 direction of propagation; positive direction pointing away from the source/origin of the dispersive
 166 wave); and the transverse component $t(t)$ (in the transverse direction, obtained by rotating the radial
 167 direction clockwise by $(\pi/2)$, as shown in Figure 2). To derive an expression to directly compute θ , we

168 start by relating the horizontal components u_x and u_y to the components u_r and u_θ as
 169 follows:

$$(7)$$

170 If the radial component u_r and the shifted (Hilbert Transformed) vertical component u_θ are in
 171 phase, then we can reasonably consider that these are the components of a Rayleigh wave, which, in
 172 turn, implies that, the correlation coefficient of the transverse component u_x and u_y should ideally
 173 be zero (in essence we are assuming that the identified Rayleigh wave is not correlated with the linearly
 174 polarized wave in the transverse direction, if such a wave exists). Under this assumption, Eq. (5) leads
 175 to:

$$(8)$$

176 Substitution of the second equation given in (7) in the above expression leads to:

$$(9)$$

177 Solving this equation for θ we obtain the average direction of propagation of the wave train:

$$\theta = \arctan\left(\frac{u_y}{u_x}\right) \quad (10)$$

178 where the subscript θ is added because Eq. (10) provides only the ‘reference’ angle of the direction of
 179 propagation of the Rayleigh waves. The azimuth θ in its correct quadrant can be computed with the
 180 expressions:

(11)

181 which can be condensed in the following single equation:

(12)

182 where $\text{sgn}(\cdot)$ is the sign function. Note that Eqs. (11) and (12) take into account the sign of reference
183 angle θ , which will have the same sign as θ . If the extracted signal is composed of more than one
184 dispersive wave propagating in distinct, albeit similar, directions, then, Eq. (10)-(12) should be applied
185 independently to each one of them. By inspecting the Stockwell Transform of the signal the analyst can
186 observe if there are several wave trains.

187 The time-domain procedures to compute the direction of propagation of Rayleigh waves presented in
188 this section work well if the waves have already been identified and extracted. An implicit assumption in
189 those procedures is that Rayleigh waves are either pro-grade or retro-grade, but not a mixture. Retro-
190 grade particle motion is usually the type of polarization expected for Rayleigh waves. However, some
191 geological settings allow for the generation of both retro-grade and pro-grade waves. One example is the
192 West Coastal Plain in Taiwan, as reported by Wang *et al.* (2006). With the IRE criterion as defined in
193 Eq. (2) it is not possible to identify whether the particle motion is pro-grade or retro-grade. Galiana-
194 Merino *et al.* (2011) suggest the instantaneous phase difference between the Radial and Vertical
195 components can be used to discern between these two types of motion. However, this requires
196 knowledge of the angle specifying the radial direction, and in most cases this angle is not available to
197 the analyst. This is why we propose a new criterion to filter the components of the signal to extract
198 Rayleigh waves, which does not require the specification of their direction of propagation, and

199 differentiates between pro-grade and retro-grade motion. This criterion is the Normalized Inner Product
200 (NIP) that we define in the following section.

201 **THE NORMALIZED INNER PRODUCT**

202 Let the Stockwell Transforms of the North, East and Vertical components of the signal be denoted by
203 S_N , S_E , S_V , respectively. In a similar manner, we denote the Stockwell Transforms of
204 the radial and transverse component of the signal by S_R and S_T . We recognize that each of
205 the discrete Stockwell Transforms is a matrix defined in the discretized z space. Furthermore, each
206 element S_{ij} , of the discretized space is a complex number and may be expressed as
207 follows:

(13)

208 We find it convenient to treat each element S_{ij} as a two-element vector; *e.g.* for the vertical
209 component S_V , we define:

(14)

210 with corresponding definitions for the radial, transverse, North and East components, S_R , S_T ,
211 S_N , S_E , respectively. Once we treat each element of the discretized z space as a vector, we
212 can define inner (dot) products with them. For example, the inner product of the radial with the vertical
213 component can be expressed as:

(15)

214 The inner product allows one to take advantage of the following facts: 1) the phase of the
 215 Stockwell Transform is absolutely referenced, (2) when normalized, the inner product is (in a way) the
 216 time-frequency counterpart of the correlation in the time domain. Therefore, for a Rayleigh wave, if we
 217 shift appropriately (i.e. by a phase-delay for pro-grade particle motion, or by phase-advance for retro-
 218 grade particle motion) the vertical component, then the shifted vertical component should be in-phase
 219 with the radial component. If we refer to the shifted vertical component by V_{shifted} , then ideally
 220 $V_{\text{shifted}} = V_{\text{radial}}$, and $V_{\text{shifted}} = V_{\text{vertical}}$. Practically, we expect the difference
 221 $|V_{\text{shifted}} - V_{\text{radial}}|$ to be small and, consequently, we expect $V_{\text{shifted}} = V_{\text{radial}}$ to attain
 222 values close to 1. Making use of the definitions established earlier, the Normalized Inner Product of the
 223 radial and appropriately shifted vertical components, denoted by NIP is given by:

$$\text{NIP} = \frac{\int V_{\text{shifted}} V_{\text{radial}} dt}{\sqrt{\int V_{\text{shifted}}^2 dt \int V_{\text{radial}}^2 dt}} \quad (16)$$

224 Note that in the time-frequency domain, the time shifted vertical component is obtained simply
 225 by multiplying the positive frequencies of V_{vertical} by $e^{-i\omega\tau}$ for a phase advance, and by
 226 $e^{i\omega\tau}$ for a phase delay. Then, we can construct simple filters to retain only those regions in the
 227 space where the value of the NIP is close to 1 (say, $\text{NIP} > 0.9$) and setting the rest of the
 228 space equal to zero. Following Pinnegar (2006), the filters can be alternatively defined using
 229 continuous functions by means of cosine tapers, to reduce numerical artifacts when the filtered
 230 transforms are inverted to recover the extracted waves.

231 Since we do not know the direction of propagation of the Rayleigh wave, the elements NIP cannot
 232 be computed directly applying the Stockwell Transform to some time history in such direction. Here we

233 propose an indirect method to compute the elements . Exploiting the linearity of the Stockwell

234 Transform, we obtain the time-frequency counterpart of Eq. (7):

(17)

235 In order to find the azimuth , we again make use of the fact that, for a Rayleigh wave, the correlation

236 between the transverse component and the shifted vertical component is zero:

(18)

237 Following a similar reasoning to the one presented in the previous section, the time-frequency

238 counterpart of Eq. (10) can be expressed as:

$$\text{-----} \quad - \quad - \quad (19)$$

239 Here is a function of , and is expected to present small variations when associated to a wave

240 train. If several wave trains are present in the signal, having different directions of propagation, Eq. (19)

241 is valid for each of the corresponding time intervals. Now, taking in consideration the quadrants in the

242 N-S, E-W plane, the azimuth giving the direction of propagation of the wave train is given by:

$$- \quad (20)$$

243 where

(21)

244 and θ if the sense of propagation of the wave train is towards the East, whereas
245 θ if the sense of propagation of the wave train is towards the West. The determination of
246 the sense of propagation can be accomplished if the position of the source/origin of the signal is known,
247 or if we have more than one station recording the propagating dispersive wave. Let us emphatically note
248 that if the sense of propagation, of the phase under investigation, is not established, pro-grade or retro-
249 grade motion cannot be defined without ambiguity. Also, let us note that sense of propagation and
250 direction of propagation are not the same thing. The direction is given by a numerical value of θ ,
251 whereas the sense of propagation only indicates whether the propagation of the wave train is towards the
252 East or the West. Once the angle θ is computed, the elements α can be computed in the
253 time-frequency domain with the first equation given in (17).

254 The NIP criterion is particularly useful when in the seismogram we have simultaneously the traces of
255 pro-grade and retro-grade Rayleigh waves. These waves may be associated with different frequencies if
256 the physical processes that generate them are different. Since the NIP criterion we use is defined in
257 terms of θ , the filter constructed with this criterion will exclude the regions of the ω - θ space
258 that are associated with pro-grade particle motion if θ has been obtained with a phase advance.
259 Conversely, the filter will exclude the regions of the ω - θ space corresponding to retro-grade motion if
260 θ has been obtained with a phase delay (Figure 1).

261 After the filters are applied to the time-frequency components of the signal, the filtered Stockwell
262 Transforms are inverted and what we eventually obtain are Rayleigh waves with only pro-grade or retro-
263 grade particle motion (depending on how we shifted the vertical component). The radial, transverse and
264 vertical components can then be obtained by either of the following two approaches:

265 1) Applying the filter to the u , v and w components, and inverting the resulting
 266 Transforms to obtain the North-East-Vertical components of the extracted wave train. Then, the radial-
 267 transverse components are obtained by rotation of the North-East components with the azimuth
 268 calculated with Eq. (12).

269 2) The filter is applied to the u , v and w components. Let us recall that the
 270 and w components are computed with Eq. (17). The time-domain radial and transverse
 271 components of the wave train are obtained directly by inverting the filtered Transforms.

272 **Extraction of Love Waves**

273 The ϵ criterion is also useful for the extraction of Love waves, which are dispersive waves
 274 linearly polarized on the horizontal plane along a direction which is transverse to the direction of
 275 propagation. In the case of a noise-free synthetic signal which consists of only linearly polarized waves
 276 on the horizontal plane, ϵ would be zero and apparently Eq. (19) could not be used. However if
 277 we express Eq. (19) in the following manner:

$$\frac{1}{\epsilon} = \frac{1}{\epsilon} \frac{1}{\epsilon} \tag{22}$$

278 which can be simplified as:

$$\frac{1}{\epsilon} = \frac{1}{\epsilon} \tag{23}$$

279 Thus, the computation of ϵ is not affected by the zero amplitude of w . If we consider also
 280 that for this particular case the phase of w is also zero, then Eq. (23) becomes:

(24)

281 Therefore, in this case is going to provide the *direction of polarization* of the Love wave, not its
282 direction of propagation. The wave trace is going to be found in the radial component computed
283 with Eq. (17). Now, in the case of real data we can reasonably argue that if for no other
284 reason but for the presence of ambient noise. If in fact this is the case, then Eq.(18) can be used and,
285 along with Eqs.(19) & (20), provides an estimate of the *direction of propagation* of the Love wave. In
286 this case the wave trace is going to be found in the transverse component .

287 WAVE EXTRACTION USING SYNTHETIC SIGNALS

288 In this section, we illustrate the application of our proposed procedure to extract waves from synthetic
289 signals. We consider an example very similar to the one presented by Galiana-Merino *et al.* (2011),
290 where a constructed synthetic signal is used. To construct the synthetic signal we combine three
291 windowed sinusoids with frequencies: 5, 2 and 1 Hz, shown in Figure 3, and denoted by , ,
292 and , respectively. In order to include elliptically polarized waves, we apply a phase advance of $\pi/2$
293 rad to the signal , and a phase delay of $\pi/2$ rad to the signal . The resulting signals are denoted
294 by and , respectively. The three frequencies are then combined as shown in shown in Figure
295 4, to obtain a three-component signal, which is simultaneously linearly and elliptically polarized. As
296 Figure 4 indicates, we choose the pro-grade wave of 1 Hz to be in the - plane, with following
297 components: in the -direction, and in the -direction. On the other hand, the retrograde
298 wave of 2 Hz is assigned to the - plane, with the following components: in the -direction

299 and in the z -direction. In the x - y plane we choose to have a linearly polarized wave of 5 Hz
300 defined as $u = v$ in both x and y directions. Since both the u and v components have the same
301 amplitude, the linearly polarized wave has a direction of propagation of 45 degrees measured clockwise
302 from the positive x -axis.

303 Now, we translate the x - y coordinate system into a North-East-Vertical system. For this, we assign an
304 azimuth of 60 degrees (measured clockwise from North) to the retro-grade wave (which propagates
305 along the z -axis). Using a right-handed coordinate system, the direction of the other two waves will then
306 be as follows: the azimuth of the pro-grade wave (which propagates along the x -axis) will be 150
307 ($=60+90$) degrees, and the azimuth of the wave linearly polarized in the x - y plane will be 105 ($=60+45$)
308 degrees. We then rotate the x and y components to obtain the North-East components by means of the
309 rotation matrix:

(25)

310 The resulting N - E - V components are shown in Figure 5. We can observe the three frequencies are
311 superimposed and there is no visual indication of the type of waves contained in the signal. We will
312 work with these components as starting data for our proposed procedures, since most available
313 seismograms are given in N - E - V components.

314

315 **Extraction of Retro-grade Rayleigh wave**

316 In this section we will apply filtering to extract the retro-grade wave, that is, the 2-Hz elliptically
317 polarized wave in the y - z plane. We will use both, the IRE, and independently, the NIP, as criteria to

318 construct and compare the filters. Once the wave is extracted we will recover the azimuth that was
 319 assigned to the retro-grade wave in the previous section. We start by computing the Stockwell
 320 Transform of the $N-E-V$ components, whose amplitudes are shown in Figures 6(a)-(c). Using the
 321 notation introduced in the previous section, \hat{N} , \hat{E} , and \hat{V} ,
 322 \hat{N} . Figures 6(a)-(c) illustrate that, as expected, most of the energy of the linearly polarized wave
 323 is contained in the East component, whereas for the elliptical polarized wave, most of the energy is
 324 contained in the vertical component. With the Transforms of the $N-E-V$ components, and using Eqns.
 325 (19)-(21), we compute the angle θ , shown in Figure 6(d). Because of the color scale distributed in
 326 the time-frequency space, we cannot observe exactly the value of the azimuth for each frequency in
 327 Figure 6(d), however, we can affirm that the azimuth is close to 100 degrees for the 5 Hz wave (we have
 328 assigned 105 degrees in the previous section), 60 degrees for the 2 Hz wave, and 150 degrees for the 1
 329 Hz wave. The exact values of the azimuth for each frequency will be provided after we extract each
 330 wave, as it will be shown in the sequel. Now, with the computed angle θ , we use equation (17) to
 331 compute the \hat{R} and \hat{T} components. The results are shown in Figures 6(e)-(f). We can
 332 observe that there is no energy in the transverse component for all frequencies. This is an expected result
 333 because the angle θ is derived under the assumption that the correlation between the transverse and
 334 vertical components is zero. It is important to clarify that when we compute the \hat{R} component
 335 using \hat{N} , each frequency is rotated according to its corresponding θ . The obtained “radial
 336 component” in the full time-frequency space will not have the physical meaning of the Stockwell
 337 Transform of a component of the signal in a specific “radial” direction. However, such computation is
 338 useful for extracting waves, since after we apply filtering, only one wave (or wave train) will remain in
 339 the time-frequency domain, and with it, only one direction of propagation. The next step is the
 340 computation of NIP \hat{R} , obtained by applying equation (16) and shown in Figure 7(a). Since we want

341 to extract the wave with retro-grade motion, we set ϵ . The red region in Figure 7(a)
 342 corresponds to the presence of the retro-grade wave (the NIP ϵ), whereas the black region
 343 corresponds to the pro-grade wave (the NIP ϵ). For the linearly polarized wave, the values of
 344 NIP ϵ oscillate around zero. This unstable behavior [not shown in figure 7(a)] is due to the presence
 345 of the amplitude of A in the denominator in Eq. (16); the amplitude of A is zero for a wave
 346 linearly polarized in the $x-z$ plane. This situation, however, is unlikely to be found in real seismograms
 347 because the presence of noise will keep the amplitude of A different from zero. Then, in order to
 348 avoid this unstable behavior when dealing with noise-free synthetic signals, the amplitude A used
 349 in Eq. (16) may be modified in the following manner:

$$(26)$$

350 where ϵ is the tolerance for small values of A . Because of the finite energy
 351 carried by seismic waves, we expect A to be bounded. In Figure (7a) the ϵ is computed
 352 adopting a tolerance ϵ . Now, for comparison, the IRE is also shown in Figure 7(b), which was
 353 obtained by applying equations (2)-(4). We can observe that the regions corresponding to both the pro-
 354 grade and retro-grade wave have an IRE of about 0.5. As expected, the IRE is zero in the region of the
 355 linearly polarized wave.

356 Now that the waves have been identified, we construct filters to isolate or extract the elliptically
 357 polarized (retro-grade) wave. The continuous filters based on the NIP ϵ and the IRE are constructed
 358 as follows:

359 where θ is the threshold value, and $\Delta\theta$ the width of the cosine taper. In this example we selected,
 360 $\theta = 0.1$, $\Delta\theta = 0.05$, and $\Delta\theta = 0.05$ to construct the filter using as criterion the value of the IRE. On
 361 the other hand, for the filter using as criterion the value of the NIP, we selected $\theta = 0.1$,
 362 $\Delta\theta = 0.05$, and $\Delta\theta = 0.05$. Since we already computed the component u_{θ} , the filters can be applied to it,
 363 and to the vertical component u_z to extract directly the Rayleigh waves. In Figures 7(c)-(d) we
 364 compare the filtered component u_{θ} using the NIP criterion [Figure 7(c)], and the IRE
 365 [Figure 7(d)]. It is evident that filtering with the IRE criterion alone does not separate the pro-grade and
 366 retro-grade waves in this example. On the other hand, Figure 7(c) shows the effectiveness of the
 367 NIP criterion to isolate the retro-grade (Rayleigh) waves present in the synthetic signals.

368 Finally, the desired wave is extracted by computing the inverse Stockwell transforms after the u_{θ} ,
 369 u_z and u_y components are filtered with the NIP criterion. Figure 8 shows the radial,
 370 transverse and vertical components of the unfiltered signal and those of the extracted wave in the time
 371 domain. In the previous section we selected the y-axis as the direction of propagation of the retro-grade
 372 wave, and thus, the y-axis is the “radial” direction for this wave. As expected, there is no extracted wave
 373 in the transverse direction (the pro-grade wave which would have appeared on the transverse component
 374 has been eliminated by filtering).

375 Let us note that we use θ to compute the NIP, and then we use the NIP to *filter* and
 376 *extract* the desired wave. However, even though the components of the extracted wave are already
 377 obtained in the radial and transverse direction, the unique numerical value giving the azimuth of such

378 directions has not been provided. If such azimuth is also desired, it can be computed by filtering the
379 u , v and w components with the NIP criterion. Then, the angle α is computed
380 using Eqs. (10)-(12) once the time-domain $N-E-V$ components are obtained inverting the filtered
381 u , v and w components. The $N-E-V$ components of the extracted retro-grade wave
382 computed in this manner are shown in Figure 9. The extracted wave has a frequency of 2 Hz, as
383 expected. Now, applying Eqs. (10)-(12) to these $N-E-V$ components, we obtain an azimuth for the retro-
384 grade Rayleigh wave of 59.9994 degrees, the expected value. Let us note that the $R-T-V$ components of
385 Figures 8(d)-(f) were obtained by rotating the $N-E-V$ components of Figure 5 with the computed
386 azimuth.

387 **Extraction of Pro-grade Rayleigh Wave**

388 To extract the pro-grade Rayleigh wave from the synthetic signal we follow the same procedure as in the
389 previous section, but now we set $\phi = 180^\circ$, for a phase delay for the vertical component
390 w . We can observe in Figure 10(a) that the regions for the NIP u and the NIP
391 w have been interchanged [compare Figure 10(a) with Figure 7(a)], since now we are targeting the wave of
392 1 Hz (which, we remind the reader, is the pro-grade wave propagating along the x -axis, that is, an
393 azimuth of 150 degrees). When we apply the filter, based on the NIP criterion, to the
394 component, we can observe that the only remaining wave has a frequency of about 1 Hz, as shown in
395 Figure 10(b). Finally, the radial, transverse and vertical component of the unfiltered signal and extracted
396 wave are shown in Figure 11. Once again, there is no component in the “transverse” direction of the
397 extracted wave. The azimuth giving the direction of propagation of the pro-grade wave, obtained by
398 applying Eqs. (10)-(12) is 150.0011 degrees. As expected, in this case the “radial” direction coincides
399 with the x -axis of the coordinate system, as shown in Figure 11.

400 To verify that we in fact have extracted retro-grade and pro-grade Rayleigh waves, we inspect their
 401 polarization characteristics. In Figure (12) we compare the radial and shifted vertical components of the
 402 extracted waves. For the retro-grade, the vertical component is shifted with a phase advance, and
 403 for the pro-grade wave, with a phase delay. Since the compared components are clearly in-phase,
 404 we can conclude that we have extracted Rayleigh waves.

405 **Extraction of Linearly Polarized wave**

406 Now we consider the problem of extracting the wave that is linearly polarized in the $x-y$ plane. In such a
 407 case, Love waves and shear waves would be the candidates. For Love waves we would expect the
 408 presence of a dispersed wave train. Note that to extract the linearly polarized wave, the component u can
 409 be obtained either way, by shifting v with a phase advance, or a phase delay. In Figure (13a) the
 410 u was computed shifting v with a phase delay. We can observe that the values of the
 411 for the 5 Hz wave are close to zero, a result consistent with linear polarization. Thus, in this case the
 412 continuous filter is constructed to exclude regions of the $x-y$ plane for which $u \neq 0$, as
 413 follows:

$$u = 0 \tag{28}$$

414 where θ , ϕ and ψ . The results of applying this filter to the
 415 component are shown in Figure (13b). It can be observed that the only remaining wave in the filtered
 416 component is the wave of 5 Hz. Next, the radial, transverse and vertical components of the
 417 unfiltered signal and extracted wave are shown in Figure (14). Here the $y-x$ components of the unfiltered

418 signal have been rotated 45 degrees, to obtain its radial and transverse components. Even before filtering
 419 we can already observe that the high frequency wave is present only in the “radial component.
 420 Regarding the extracted wave, Figure (14) shoes that only the radial component of the extracted signal is
 421 non-zero, consistent with what it was anticipated. Now, in this case of a noise-free synthetic signal, Eq.
 422 (10) is not appropriate to compute the azimuth of the direction of polarization of the wave, since the
 423 time-domain component is zero. However, we can take advantage of the fact that we have already
 424 extracted the radial component of the wave. Let us note that for a wave linearly polarized on the
 425 horizontal plane:

(29)

426 if is in the direction of polarization. Thus, a new expression can be obtained, in the same manner
 427 we derived Eq. (10):

(30)

428 After computing the North and East components of the extracted wave (inverting the filtered
 429 and components) the azimuth obtained using Eqs. (30) and (12) is 105.0004. It is important to
 430 remark that this azimuth gives the direction of polarization. If the extracted wave is a Love wave, its
 431 direction of propagation would be perpendicular to it.

432 **AN EXAMPLE WITH REAL SIGNALS**

433 In this section we apply the procedure for identification and extraction of surface waves produced by an
 434 aftershock of the Chi-Chi earthquake in the West Coastal Plain (WCP) in Taiwan, which occurred on

435 September, 20th 1999 at 1803 UTC with a magnitude of M_w 6.2. This aftershock is very useful to test
436 the proposed method to extract surface waves, since it produced very strong and clear surface waves in
437 the WCP. Besides, since Rayleigh and Love waves had been previously identified from the recordings
438 and reported in the literature (e.g., Wang *et al.*, 2006) this data set allows us to assess with confidence if
439 we are in fact extracting Rayleigh and Love waves. Figure (15) shows a map with the directions of the
440 Rayleigh wave propagation obtained by Wang *et al.* (2006), where the location of the epicenter is also
441 indicated. The circle in Figure (15) specifies the location of station TCU116, which we will consider for
442 this example.

443 **Extraction of Retro-grade Rayleigh waves**

444 The $N-E-V$ components of the displacement time history at station TCU116 during the aftershock are
445 shown in Figure (16). The displacements were obtained by independently bandpass filtering between 0.1
446 and 10 Hz and integrating twice the components of the acceleration histories. We can observe from the
447 time histories in Figure (16) that most of the energy of the signal is contained in the East and Vertical
448 components. The Stockwell Transforms of the displacements histories are computed, and with them, we
449 compute the angle using Eqs. (19)-(20). Then, the components and are
450 computed according to Eq. (17). The results are shown in Figure (17). In Figure 17(a) we can observe
451 regions in the time-frequency domain (between 20 and 50 seconds) with small variations of the values of
452 , which can be associated to wave trains. We find very little energy in the component,
453 even in this case of a real signal, since is derived under the assumption of zero correlation
454 between the and components. The next step is the computation of NIP , obtained
455 by applying equation (16) and shown in Figure 18(a). Since we want to extract Rayleigh waves with
456 retro-grade motion first, . Figure 18(a) shows that using the NIP we can

457 identify the regions of the k_x plane where the components u and v are best correlated.
458 The region corresponding to the retro-grade motion is indicated by the red color. For comparison, the
459 IRE is also shown in Figure 18(b). We can conclude from the comparison that the NIP is more
460 stable over the k_x domain, as opposed to the IRE, which has more variation in the Stockwell
461 transform domain. In Galiana-Merino *et al.* (2011), it is even stated that a 2D filter needs to be applied
462 to the IRE obtained with the SWPD, because its high variation could lead to numerical problems. In this
463 example, since we are not dealing with synthetic signals, the NIP is computed with Eq. (16)
464 without making any modification to \hat{u} , and without any smoothing.

465 Figure 18(c) shows the u component filtered with the NIP criterion, according to Eq. (27).
466 The same component filtered with the IRE criterion is shown in Figure 18(d). The results of this
467 example clearly demonstrate that filtering with the NIP criterion effectively isolates the retro-
468 grade wave from the pro-grade wave. Upon inverting the filtered transforms, we obtain the extracted
469 retro-grade wave. In Figure (19) we can observe the radial, transverse and vertical components of the
470 unfiltered signal and the extracted retro-grade wave. The comparison between the unfiltered signal and
471 extracted wave shows that filtering has excluded a wave component observed between 25 and 35
472 seconds. Such component would not have been excluded filtering with the IRE criterion alone. We can
473 also observe that the transverse component of the extracted wave is minimized. The correlation
474 coefficient computed as in Eq. (5) between the radial and shifted (with a phase advance) vertical
475 components of the extracted wave is 0.91097, showing in a quantitative manner the good results that are
476 obtained when the NIP criterion is used. Finally, the azimuth of the direction of propagation of the
477 Rayleigh wave is computed with Eqs. (10)-(12), obtaining a value of 257.9926 degrees. This result is
478 compatible with the directions reported by Wang *et al.* (2006), indicated in Figure (15). The angle of

479 257.9926 degrees was used to rotate the *N-E-V* components of the unfiltered signal to obtain the
480 components *R-T-V* components shown in Figures 19(a)-(c).

481 **Extraction of Pro-grade Rayleigh waves**

482 Figure 20(a) shows NIP to extract the pro-grade Rayleigh waves, and Figure 20(b) shows the
483 component when filtered with this criterion. We observe that the pro-grade wave train has
484 different frequency content (higher frequencies) than that of the retro-grade wave train, and that it is
485 located at around 30 seconds. Figure 21 shows the radial, transverse, and vertical components of the
486 unfiltered signal and extracted pro-grade wave. We can observe the different time location of the pro-
487 grade wave relative to the previously extracted retro-grade wave. With the use of the NIP criterion, we
488 have managed to separate these waves, even in the time range in which they overlap. Certainly, such
489 separation is possible because of the different frequency content of the waves. The correlation
490 coefficient of the radial and shifted (with a phase delay) vertical components of the extracted pro-grade
491 wave is 0.91034. The computed azimuth is 282.6976 degrees. This azimuth is significantly different
492 from the one obtained for the retro-grade waves (257.9926 degrees), indicating that probably the
493 observed pro-grade and retro-grade Rayleigh waves are generated in different manners.

494 Finally Figure (22) shows the comparison between the radial and shifted vertical components of the
495 extracted Rayleigh waves. Clearly, the radial component and the vertical component shifted with a
496 phase advance shown in Figure 22(a) are in phase, confirming the extracted waves of Figure 22(a) are
497 retro-grade Rayleigh waves. In Figure 22(b) the vertical component is shifted with a phase delay,
498 confirming that the extracted wave shown in Figure 22(b) is a pro-grade Rayleigh wave.

499 **Extraction of Love waves**

500 In Figure (17) we can observe that the component at station TCU116 does not show the
501 presence of a wave train that can be associated to Love waves. This is why we analyze the recording of
502 the same event at station TCU118, for which Wang *et al.* (2006) had already identified Love waves. For
503 this station we first extract the retro-grade Rayleigh wave train, following the procedure detailed in the
504 previous section. The components of the extracted retro-grade Rayleigh wave are shown in Figure 23(a).
505 Let us note that the resulting azimuth giving the direction of propagation of the retro-grade Rayleigh
506 wave train is 304.51 degrees, a result close to the 297 degrees reported in Wang *et al.* (2006). With this
507 direction we use Eq. (7) to compute the radial and transverse components of the unfiltered signal in the
508 time domain, and then compute their Stockwell Transforms, which are shown in Figure (24). A wave
509 train with a later arrival time (relative to the Rayleigh wave's arrival) is clearly present in the time-
510 frequency transverse component of the unfiltered signal, as shown in Figure 24(b). The Love waves are
511 effectively extracted using the filter based on the criterion defined in Eq. (27). Even though
512 we could use the criterion and construct a filter according to Eq. (28), the filter given in Eq.
513 (23) is more convenient because the is more stable in the space. The extracted Love
514 waves are shown in Figure 23(b). The waveforms and corresponding arrival times of the waves
515 extracted with our proposed procedure are similar to those reported in Figure 9 of Wang *et al.*, (2006).

516 Now, to illustrate the performance of our procedure to extract surface waves in high noise conditions,
517 we analyze the recording at station CHY107. This station is located farther from the epicenter, to the
518 south of the WCP, as shown in Figure 15. The strength of the wavefield at such far location is weak. A
519 comparison of the unfiltered signal and the results of applying filtering using the NIP criterion are
520 shown in Figure 25. We can observe that much of the noise has been filtered out when the NIP criterion
521 is used. The correlation coefficient between the radial and shifted vertical components is 0.8449, giving

522 a strong indication that the extracted (retro-grade) wave in the radial direction is a Rayleigh wave. This
523 high correlation is illustrated in Figure 25(d), which shows the comparison of the radial and phase
524 advanced vertical component. Furthermore, the azimuth obtained with the extracted waves is 226.22
525 degrees, a direction consistent with the location of station CHY107 relative to the epicenter, shown in
526 Figure 15. We can also observe a strong intensity (relative to the radial component) in the transverse
527 component of the extracted waves. Even though we could consider the extracted waves in this transverse
528 component as Love waves, the extracted signal might as well be simply linearly polarized noise. In cases
529 like this, with a relatively lower signal-to-noise ratio, better results can be obtained if the signal is
530 denoised before applying filtering to extract Love waves.

531 Finally, we have applied the NIP criterion to extract Rayleigh and Love waves to other stations at the
532 WCP in Taiwan. Figure 26 illustrates the extracted retro-grade and pro-grade Rayleigh waves at each
533 station. The Love waves, extracted from the transverse component of the retro-grade Rayleigh waves are
534 shown in Figure 27. The results show the extraction method is stable when applied to this dataset of
535 seismic time histories. The computed azimuths of retro-grade Rayleigh wave propagation are in
536 excellent agreement with those obtained by Wang *et al.* (2006), indicated in Figure (15).

537 **CONCLUSIONS**

538 We have proposed and developed a method to extract Rayleigh and Love waves from three-component
539 displacement histories. The proposed method, based on the Normalized Inner Product (NIP), does not
540 require *a priori* estimations of the frequency range and direction of propagation of the surface waves.
541 We have shown that the method proposed herein distinguishes between pro-grade and retro-grade
542 particle motion. Therefore surface waves with such different polarization characteristics can be more
543 easily identified. Furthermore, examples with real signals show that the Normalized Inner Product is

544 more stable over the time-frequency domain than the Instantaneous Reciprocal Ellipticity. We also
545 showed that the proposed method works well for extracting Love waves from noise-free synthetic
546 seismograms as well as from real seismograms. The method was applied to extract Rayleigh and Love
547 waves from displacement histories of aftershock 1803 of the Chi-Chi earthquake recorded at the
548 Western Coastal Plain in Taiwan. The extracted waves and corresponding directions of propagation are
549 in excellent agreement with previous surface wave analysis reported in the literature.

550 **DATA AND RESOURCES**

551 All recorded seismograms used in this work are from CD-002 titled “CWB Free-Field Strong-Motion
552 Data from Three Major Aftershocks of the 1999 Chi-Chi Earthquake: Processed Acceleration Data Files
553 on CD-ROM” prepared in 2001 by W. H. K. Lee, T. C. Shin, and C. F. Wu of the Seismological
554 Observation Center, Central Weather Bureau, Taiwan.

555 The relief geographic map of the West Coastal Plain was generated with the code READHGT written by
556 François Beauducel, from the Institute de Physique du Globe de Paris. Input data for the Digital
557 Elevation Map was downloaded from http://dds.cr.usgs.gov/srtm/version2_1. Coast lines were extracted
558 from <http://www.ngdc.noaa.gov/mgg/coast/getcoast.html>. Both websites were last accessed in January
559 2014.

560 **ACKNOWLEDGEMENTS**

561 The authors are grateful to two anonymous reviewers for constructive comments which improved the
562 clarity of the manuscript. The authors are also indebted to Dr. Fabian Bonilla for fruitful discussions on
563 surface wave propagation, and for introducing us to the use of the Stockwell transform for analysis of
564 non-stationary signals.

565 This research has been co-financed by Electricité de France (EDF) through the MARS project and by the
566 European Union (European Social Fund – ESF) and Greek national funds through the Operational
567 Program "Education and Lifelong Learning" of the National Strategic Reference Framework (NSRF) -
568 Research Funding Program: **THALES**. Investing in knowledge society through the European Social
569 Fund.

570 **REFERENCES**

- 571 Baker, G.E. and Stevens, J.L. (2004). “Backazimuth estimation reliability using surface wave
572 polarization”, *Geophysical Research Letters*, **31**, L09611, doi:10.1029/2004GL019510.
- 573 Chael, E.P. (1997) “An automated Rayleigh-wave detection algorithm”, *Bull. Seism. Soc. Am.* **87**, 157–
574 163.
- 575 Dziewonski, A., Bloch, S. and Landisman, M. (1969) “A Technique for the Analysis of Transient
576 Seismic Signals”, *Bull. Seismol. Soc. Am.*, **59**(1), 427-444.
- 577 Flinn, E.A. (1965) “Signal analysis using rectilinearity and direction of particle motion”, *Proc. IEEE*,
578 **53**, 1874–1876.

579 Galiana-Merino J.J., Parolai, S., and Rosa-Herranz, J. (2011). “Seismic wave characterization using
580 complex trace analysis in the stationary wavelet packet domain”, *Soil Dynamics and Earthquake*
581 *Engineering*. **31**(11), 1565–1578.

582 Li, X.L., Crampin S. (1991) “Complex component analysis of shear wave splitting: theory”,
583 *Geophysical Journal International*. **107**, 597-604.

584 Pinnegar, C.R. (2006). “Polarization Analysis and polarization filtering of three-component signals with
585 the time-frequency S transform”, *Geophysical Journal International*. **165**, 596–606.

586 René, R.M., Fitter, J.L., Forsyth, P.M., Kim K.Y., Murray, D.J., Walters, J.K. (1986) “Multicomponent
587 seismic studies using complex trace analysis”, *Geophysics*. **51**, 1235-1251.

588 Selby, N.D. (2001) “Association of Rayleigh waves using back-azimuth measurements: application to
589 Test Ban verification”, *Bull. Seism. Soc. Am.* **91**, 580–593.

590 Smart, E. (1978) “A Three-Component, Single-Station, Maximum-Likelihood Surface Wave Processor”,
591 *Seismic Data Analysis Center Report*, SDAC-TR-77-14, 62 pp.

592 Stockwell, R.G. (2007) “Why use the S-transform” in *Pseudo-Differential Operators: PDEs and Time-*
593 *Frequency Analysis*. (Fields Institute Communications), **52**, pp. 279–309.

594 Stockwell, R., Mansinha, L., Lowe, R. (1996) “Localization of the Complex Spectrum: The S
595 Transform”, *IEEE Transactions on Signal Processing*. **44** (4), 998–1001.

596 Vidale, J.E., (1986) “Complex polarization analysis of ground motion”, *Bull. Seismol. Soc. Am.*, **76**(5),
597 1393-1405.

598 Wang, G., Tang, G., Boore, D., Burbach, G., Jackson, C., Zhou, X., and Lin, Q. (2006). “Surface Waves
599 in the Western Taiwan Coastal Plain from an Aftershock of the 1999 Chi-Chi, Taiwan,
600 Earthquake”, *Bull. Seism. Soc. Am.* **96**, 821-845.

601 AUTHORS' AFFILIATIONS:

602 ⁽¹⁾ Universidad Nacional Autónoma de Honduras, Tegucigalpa, Honduras. E-mail:
603 kristelmeza@unah.edu.hn

604 ⁽²⁾ Department of Civil Engineering, University of Patras, GR-26500 Patras, Greece. E-mail:
605 papaga@upatras.gr


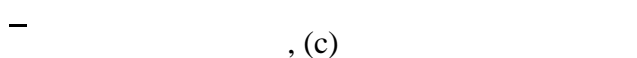

606 ⁽³⁾ Université Paris-Est, IFSTTAR, Départ. GERS, 20 Boulevard Newton, Champs sur Marne, France.
607 E-mail: jean-francois.semblat@ifsttar.fr.

608 FIGURE CAPTIONS

609 Figure 1. Time shift for vertical component. (a) For pro-grade motion (phase delay) (b) For retro-grade
610 motion (phase advance).

611 Figure 2. Reference system for direction of propagation of Rayleigh waves.

612 Figure 3. Windowed sinusoids to construct synthetic signal. (a) : 5 Hz, (b) : 1 Hz, (c) :2 Hz.

613 Figure 4. Three-component synthetic signal. (a) , (b)
614 , (c) .

615 Figure 5. Three-component synthetic signal. (a) North component, (b) East component, (c) Vertical
616 component.

617 Figure 6. Time-frequency representation of synthetic signal. (a) Amplitude of North component, (b)
618 Amplitude of East component, (c) Amplitude of vertical component, (d) Azimuth of direction of
619 propagation according to Eq. (20), (e) Amplitude of radial component (f) Amplitude of transverse
620 component.

621 Figure 7. Comparison of filtering using the IRE and NIP criteria. (a) Normalized inner product of radial
622 and phase advanced vertical component, (b) IRE computed with the three-components of the signal, (c)
623 Radial displacement component filtered using the NIP criterion, (d) Radial displacement
624 component filtered using the IRE criterion.

625 Figure 8. Rayleigh retro-grade wave extracted from synthetic signal. (a) Unfiltered transverse (-)
626 component, (b) Unfiltered radial (-) component, (c) Unfiltered (-) vertical component, (d) Extracted
627 transverse component, (e) Extracted radial component, (f) Extracted vertical component.

628 Figure 9. Extracted retro-grade Rayleigh wave. (a) North component, (b) East component, (c) Vertical
629 component.

630 Figure 10. Extraction of pro-grade wave using the NIP criterion. (a) Normalized inner product of radial
631 and phase delayed vertical component, (b) Amplitude of component filtered with the NIP
632 criterion.

633 Figure 11. Rayleigh pro-grade wave extracted from synthetic signal. (a) Unfiltered radial (-)
634 component, (b) Unfiltered transverse (-) component, (c) Unfiltered (-) vertical component, (d)
635 Extracted radial component, (e) Extracted transverse component, (f) Extracted vertical component.

636 Figure 12. Comparison of radial and shifted vertical components of extracted waves. (a) Retro-grade
637 wave (2 Hz), (b) Pro-grade wave (1 Hz).

638 Figure 13. Extraction of linearly polarized wave using the NIP criterion. (a) Normalized inner product of
639 radial and phase delayed vertical component, (b) Amplitude of component filtered with the NIP
640 criterion.

641 Figure 14. Linearly polarized wave extracted from synthetic signal. (a) Unfiltered radial component, (b)
642 Unfiltered transverse component, (c) Unfiltered vertical component, (d) Extracted radial component, (e)
643 Extracted transverse component, (f) Extracted vertical component.

644 Figure 15. Map illustrating the location of the stations on the West Coastal Plain considered in this
645 study. For some stations the arrows indicate the direction Rayleigh wave propagation estimated by
646 Wang *et al.* (2006). The star indicates the location of the epicenter of the event. The black circle
647 indicates the location of station TCU116.

648 Figure 16. *N-E-V* components of the displacement history (in cm) for Chi-Chi aftershock 1803 at station
649 TCU116. (a) North component (b) East component (c) Vertical component.

650 Figure 17. Radial and Transverse displacement components for the NIP at station TCU116. (a) Azimuth
651 of direction of propagation, (b) Amplitude of component (c) Amplitude of component.

652 Figure 18. Comparison of filtering to extract the retro-grade wave from recording at station TCU116
653 using the IRE and NIP criteria. (a) Normalized inner product of \hat{u}_r and phase advanced
654 component, (b) IRE computed with the three-components of the signal, (c) \hat{u}_r component filtered
655 with the NIP criterion, (d) \hat{u}_r component filtered with the IRE criterion.

656 Figure 19. Rayleigh retro-grade wave extracted at station TCU116. (a) Unfiltered radial component, (b)
657 Unfiltered transverse component, (c) Unfiltered vertical component, (d) Extracted radial component, (e)
658 Extracted transverse component, (f) Extracted vertical component.

659 Figure 20. Extraction of pro-grade Rayleigh wave from recording at station TCU116. (a) Normalized
660 inner product of \hat{u}_r and phase delayed \hat{u}_t component, (b) Amplitude of \hat{u}_r component
661 filtered with the NIP criterion.

662 Figure 21. Rayleigh pro-grade wave extracted at station TCU116. (a) Unfiltered radial component, (b)
663 Unfiltered transverse component, (c) Unfiltered vertical component, (d) Extracted radial component, (e)
664 Extracted transverse component, (f) Extracted vertical component.

665 Figure 22. Comparison of radial and shifted vertical components of extracted Rayleigh waves at station
666 TCU116. (a) Retro-grade wave, (b) Pro-grade wave.

667 Figure 23. *R-T-V* displacement components of extracted waves at station TCU118. (a) Comparison of
668 radial and shifted vertical component of retro-grade Rayleigh wave (b) Extracted (Love) wave in
669 transverse direction.

670 Figure 24. Radial and Transverse time-frequency components for unfiltered recording at station
671 TCU118. (a) Amplitude of radial component (b) Amplitude of transverse component.

672 Figure 25. Extracted waves from recording at station CHY107. (a) Unfiltered radial component, (b)
673 Unfiltered transverse component, (c) Unfiltered vertical component, (d) Extracted radial component
674 (black line) and shifted vertical component (gray line), (e) Extracted transverse component, (f) Extracted
675 vertical component.

676 Figure 26. Radial component (black solid line) and shifted vertical component (gray dashed line) of
677 extracted Rayleigh waves at different stations of the WCP plain in Taiwan. (a) Retro-grade waves, (b)
678 Pro-grade waves.

679 Figure 27. Extracted Love waves at different stations of the WCP plain in Taiwan.

FIGURES

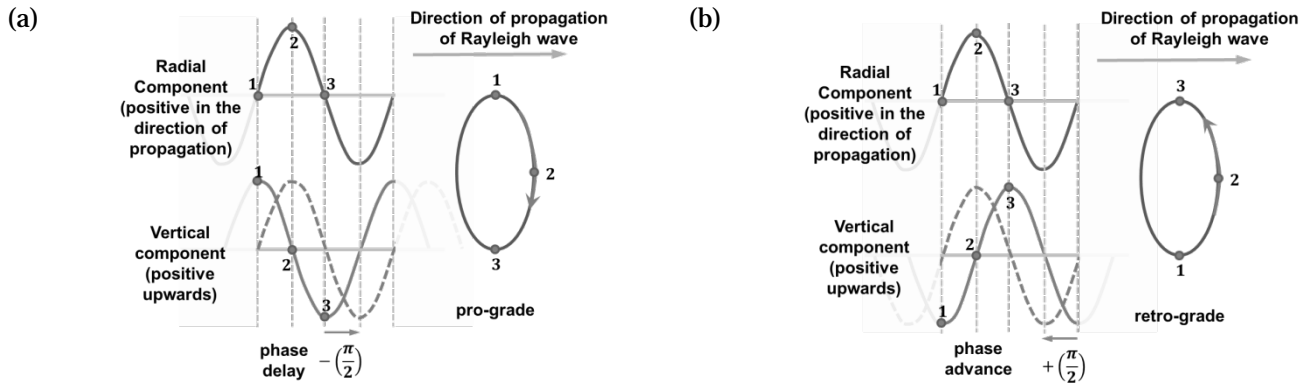


Figure 1. Time shift for vertical component. (a) For pro-grade motion (phase delay) (b) For retro-grade motion (phase advance)

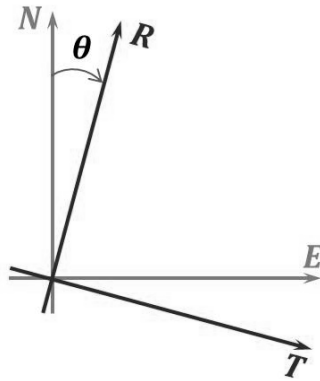


Figure 2. Reference system for direction of propagation of Rayleigh waves.

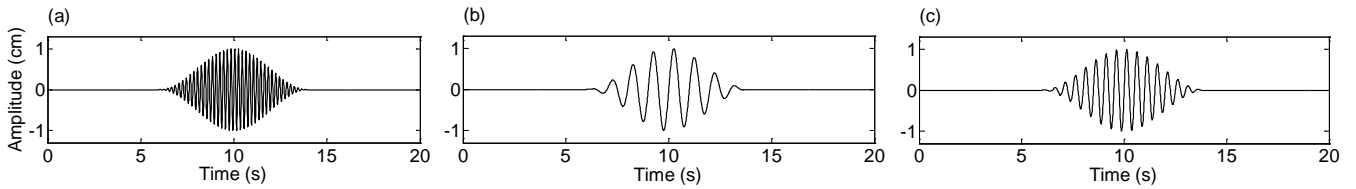


Figure 3. Windowed sinusoids to construct synthetic signal. (a) : 5 Hz, (b) : 1 Hz, (c) : 2 Hz.

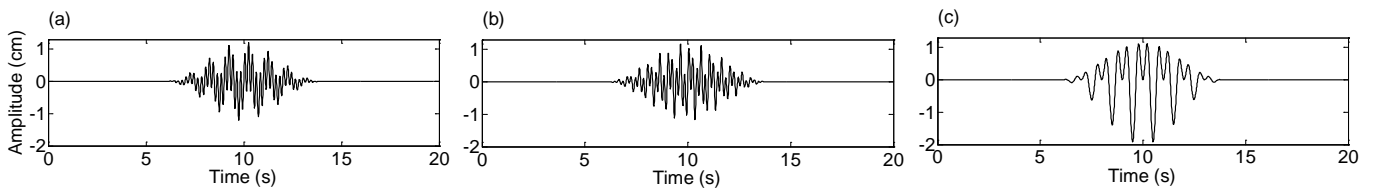


Figure 4. Three-component synthetic signal. (a) , (b) , (c) .

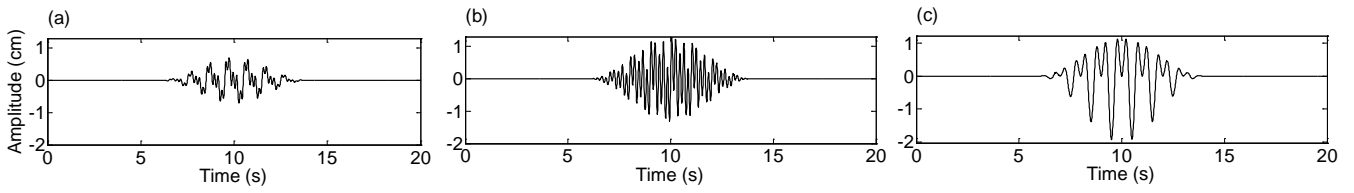


Figure 5. Three-component synthetic signal. (a) North component, (b) East component, (c) Vertical component.

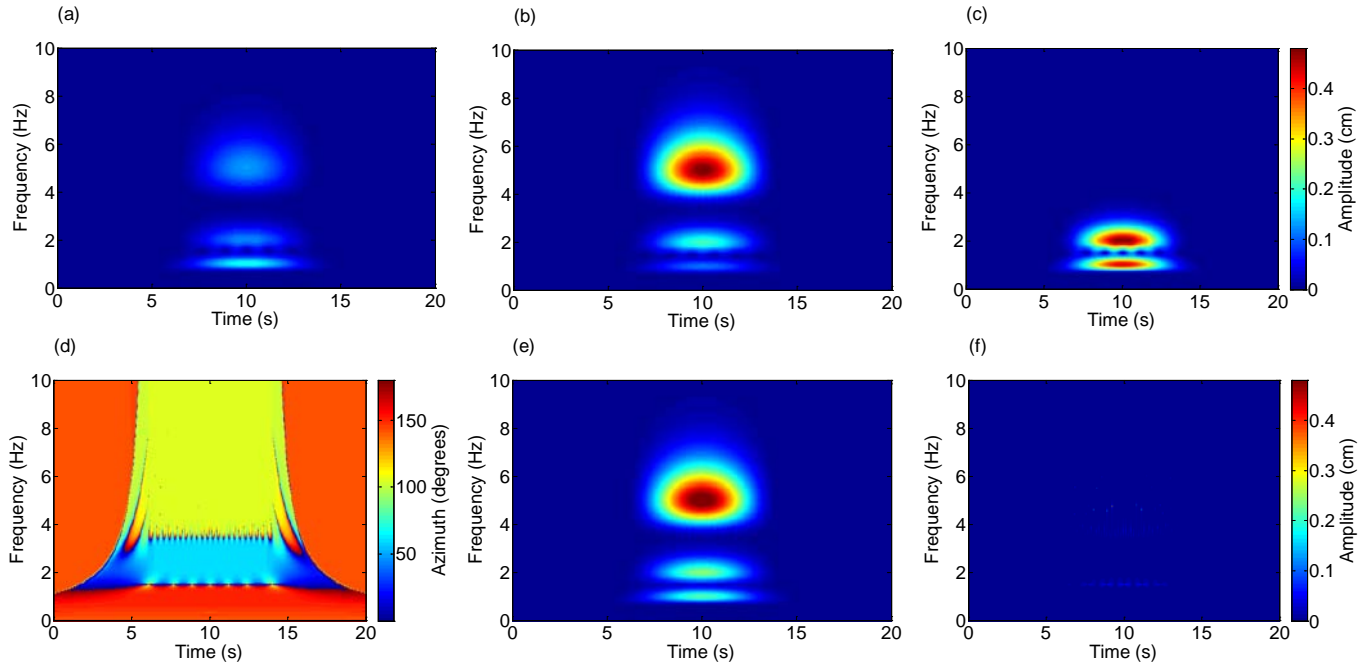


Figure 6. Time-frequency representation of synthetic signal. (a) Amplitude of North component, (b) Amplitude of East component, (c) Amplitude of vertical component, (d) Azimuth of direction of propagation according to Eq. (20), (e) Amplitude of radial component (f) Amplitude of transverse component.

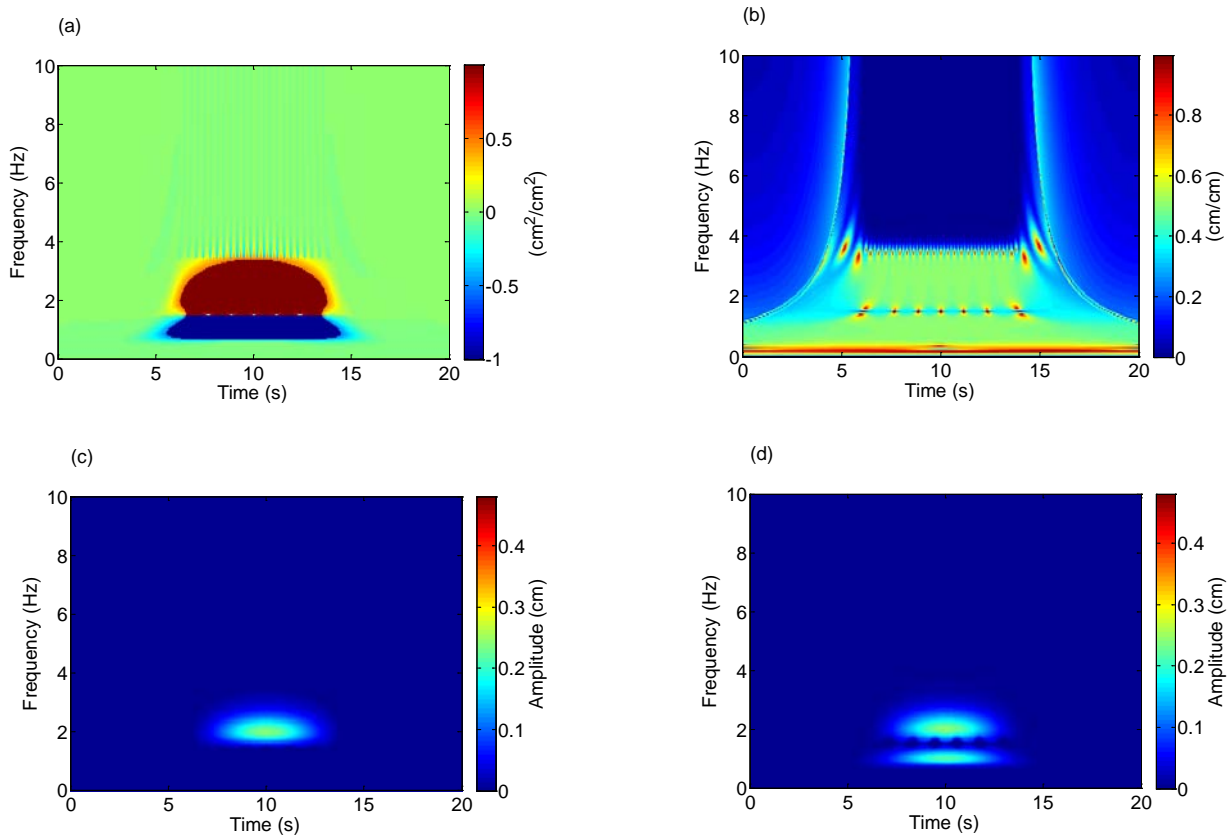


Figure 7. Comparison of filtering using the IRE and NIP criteria. (a) Normalized inner product of radial and phase advanced vertical component, (b) IRE computed with the three-components of the signal, (c) Radial displacement component filtered using the NIP criterion, (d) Radial displacement component filtered using the IRE criterion.

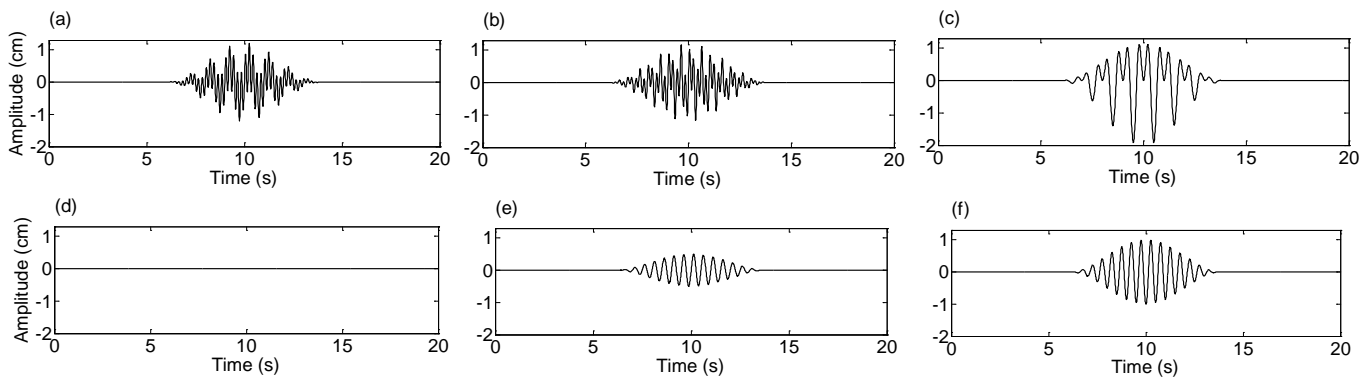


Figure 8. Rayleigh retro-grade wave extracted from synthetic signal. (a) Unfiltered transverse (-) component, (b) Unfiltered radial (-) component, (c) Unfiltered (-) vertical component, (d) Extracted transverse component, (e) Extracted radial component, (f) Extracted vertical component.

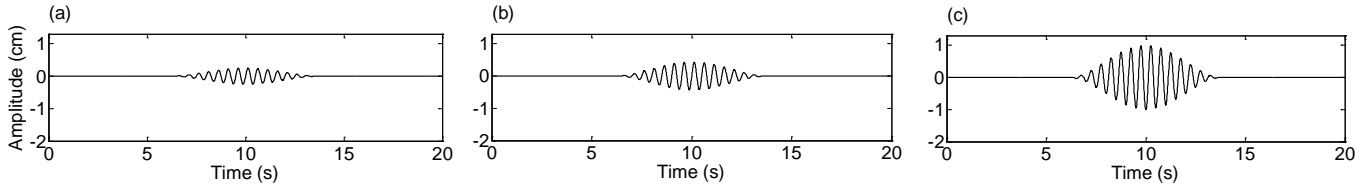


Figure 9. Extracted retro-grade Rayleigh wave. (a) North component, (b) East component, (c) Vertical component.

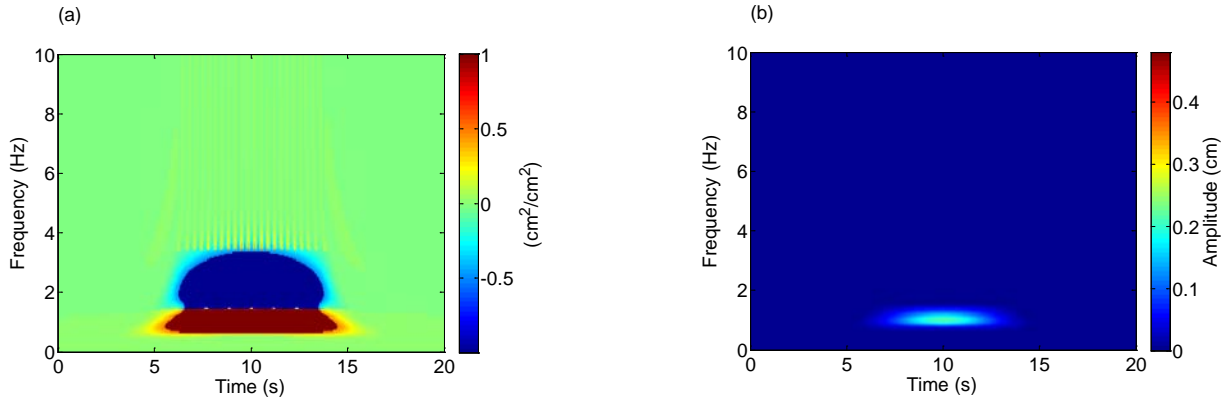


Figure 10. Extraction of pro-grade wave using the NIP criterion. (a) Normalized inner product of radial and phase delayed vertical component, (b) Amplitude of component filtered with the NIP criterion.

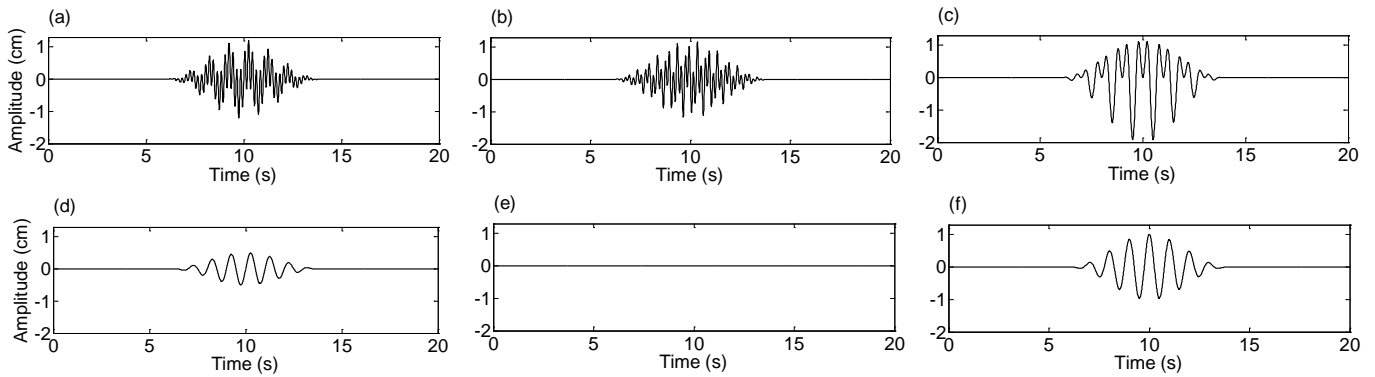


Figure 11. Rayleigh pro-grade wave extracted from synthetic signal. (a) Unfiltered radial (-) component, (b) Unfiltered transverse (-) component, (c) Unfiltered (-) vertical component, (d) Extracted radial component, (e) Extracted transverse component, (f) Extracted vertical component.

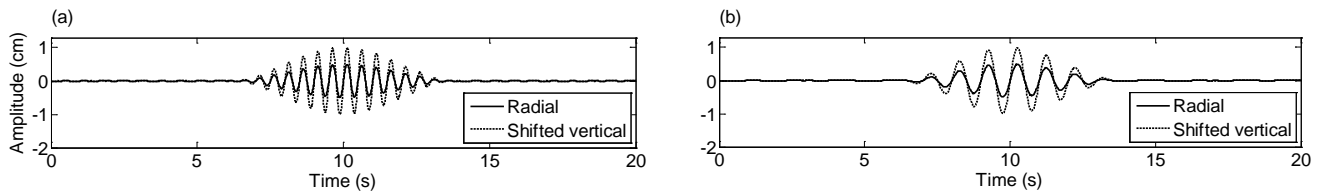


Figure 12. Comparison of radial and shifted vertical components of extracted waves. (a) Retro-grade wave (2 Hz), (b) Pro-grade wave (1 Hz).

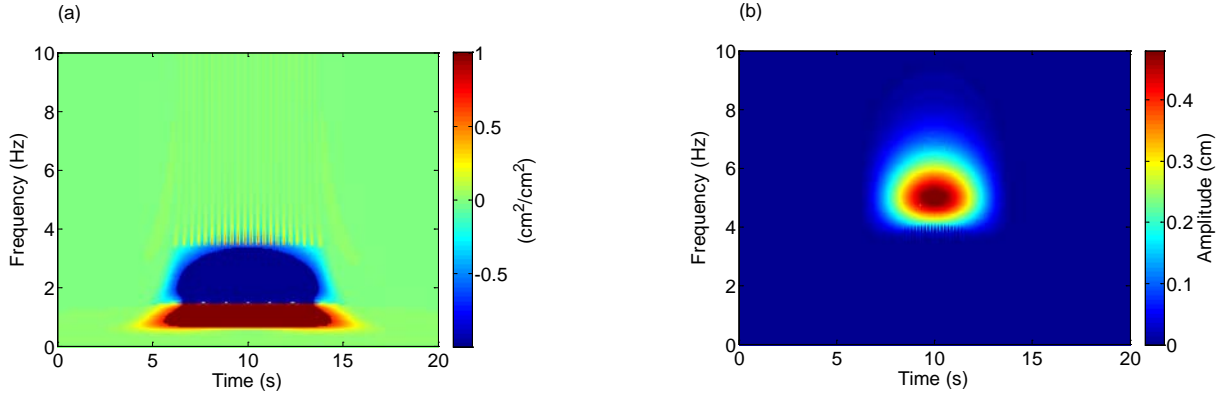


Figure 13. Extraction of linearly polarized wave using the NIP criterion. (a) Normalized inner product of radial and phase delayed vertical component, (b) Amplitude of component filtered with the NIP criterion.

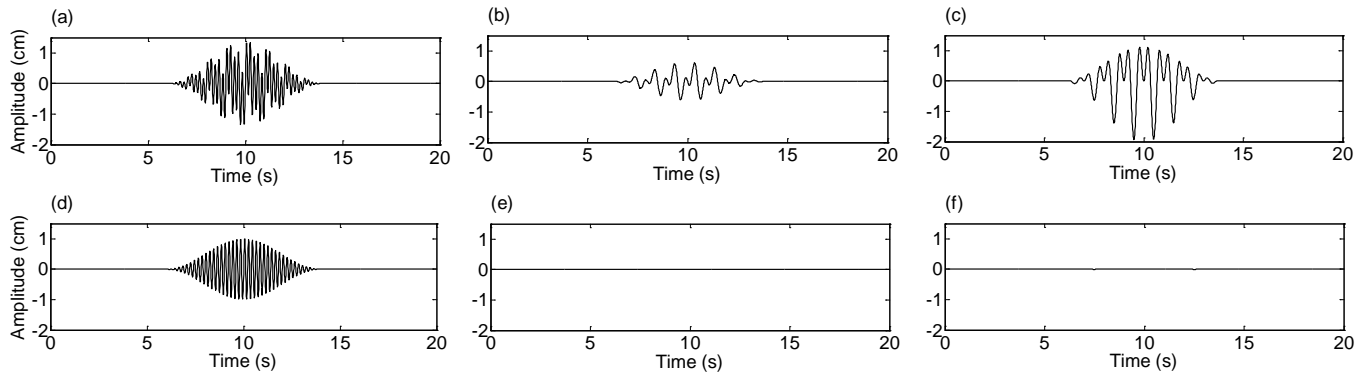


Figure 14. Linearly polarized wave extracted from synthetic signal. (a) Unfiltered radial component, (b) Unfiltered transverse component, (c) Unfiltered vertical component, (d) Extracted radial component, (e) Extracted transverse component, (f) Extracted vertical component.

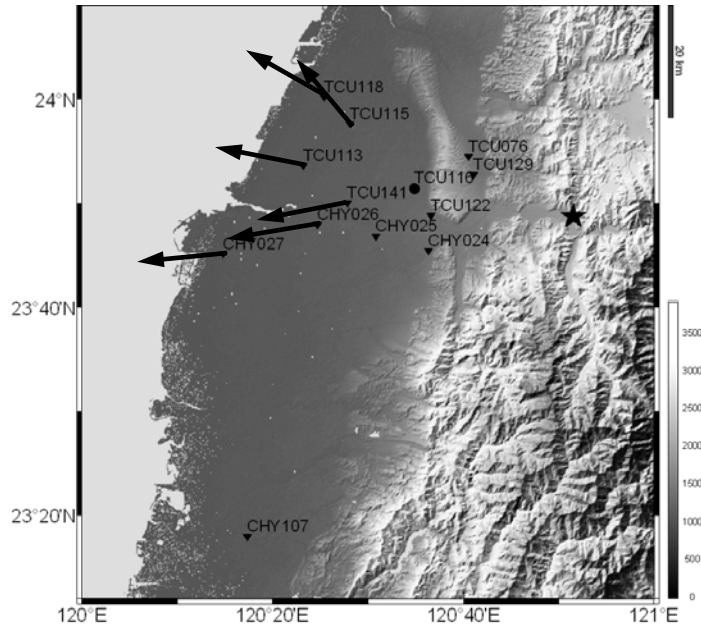


Figure 15. Map illustrating the location of the stations on the West Coastal Plain considered in this study. For some stations the arrows indicate the direction Rayleigh wave propagation estimated by Wang *et al.* (2006). The star indicates the location of the epicenter of the event. The black circle indicates the location of station TCU116.

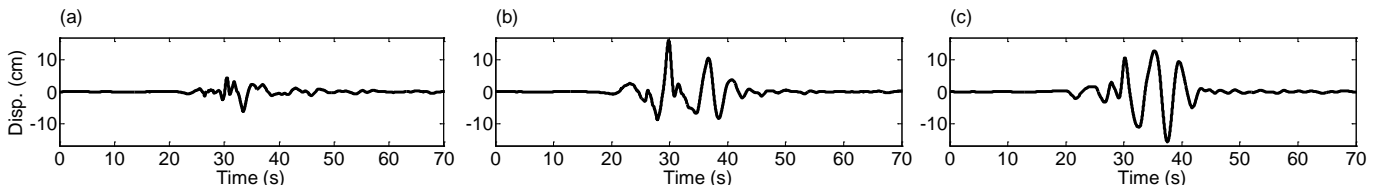


Figure 16. *N-E-V* components of the displacement history (in cm) for Chi-Chi aftershock 1803 at station TCU116. (a) North component (b) East component (c) Vertical component.

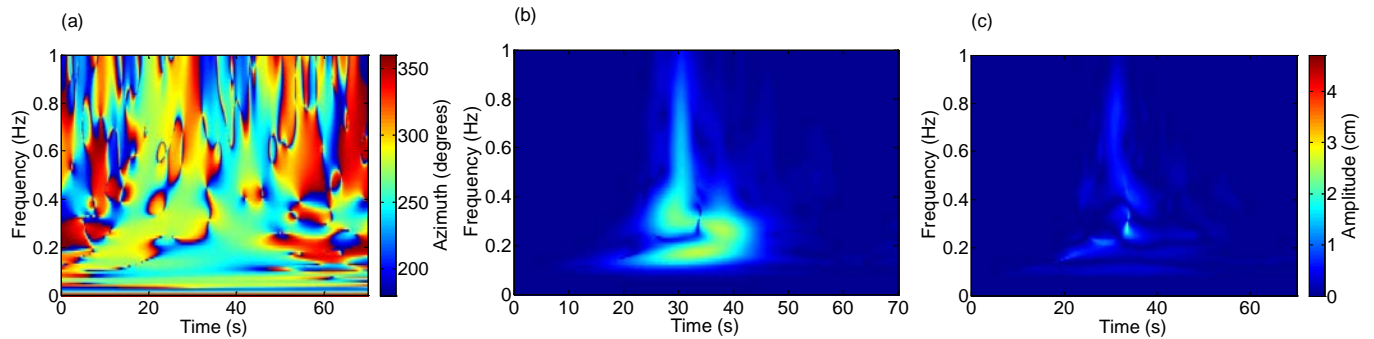


Figure 17. Radial and Transverse displacement components for the NIP at station TCU116. (a) Azimuth of direction of propagation, (b) Amplitude of radial component (c) Amplitude of transverse component.

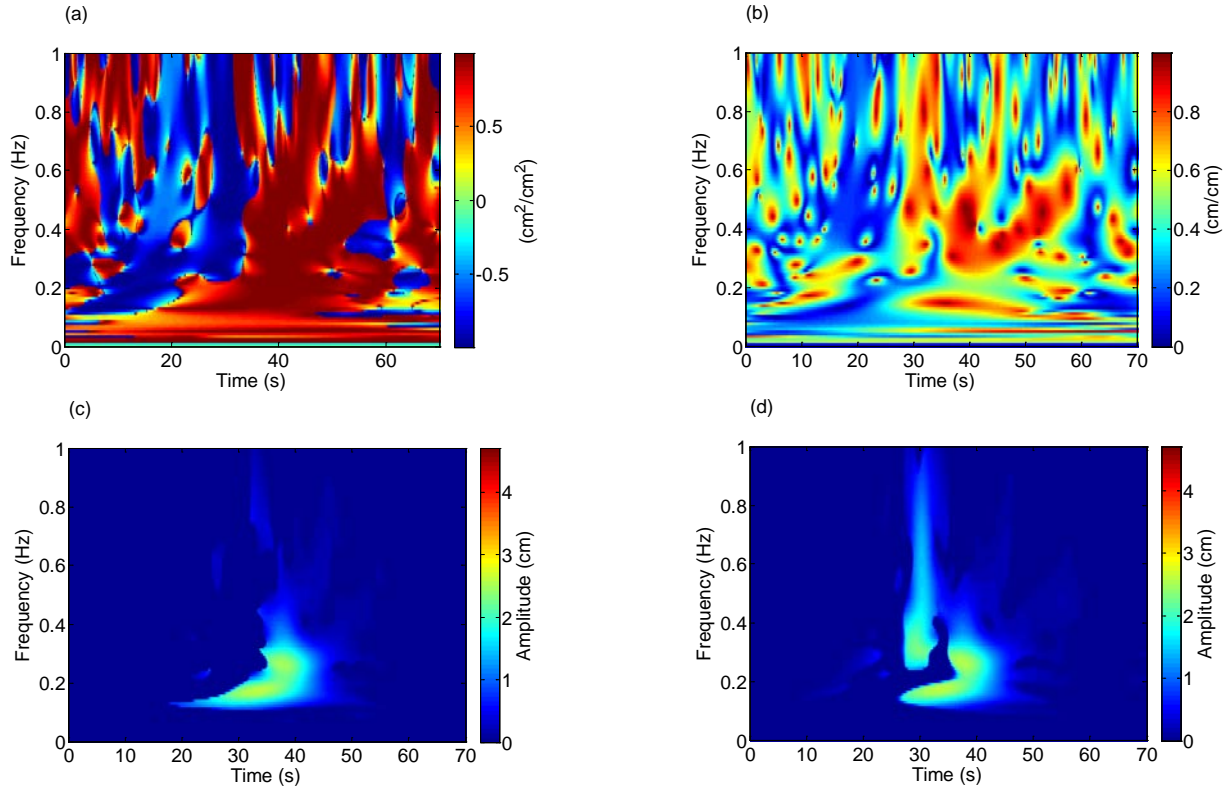


Figure 18. Comparison of filtering to extract the retro-grade wave from recording at station TCU116 using the IRE and NIP criteria. (a) Normalized inner product of the signal and phase advanced component, (b) IRE computed with the three-components of the signal, (c) component filtered with the NIP criterion, (d) component filtered with the IRE criterion.

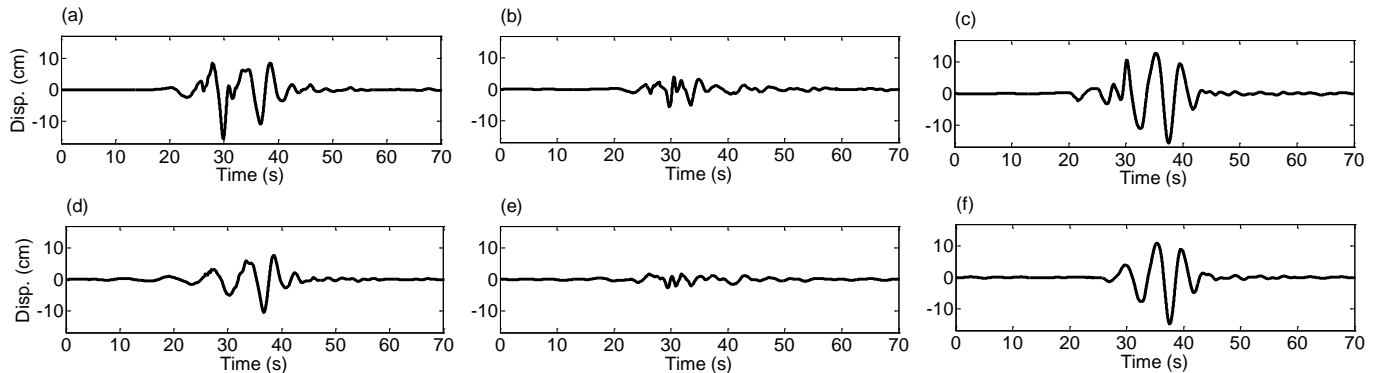


Figure 19. Rayleigh retro-grade wave extracted at station TCU116. (a) Unfiltered radial component, (b) Unfiltered transverse component, (c) Unfiltered vertical component, (d) Extracted radial component, (e) Extracted transverse component, (f) Extracted vertical component.

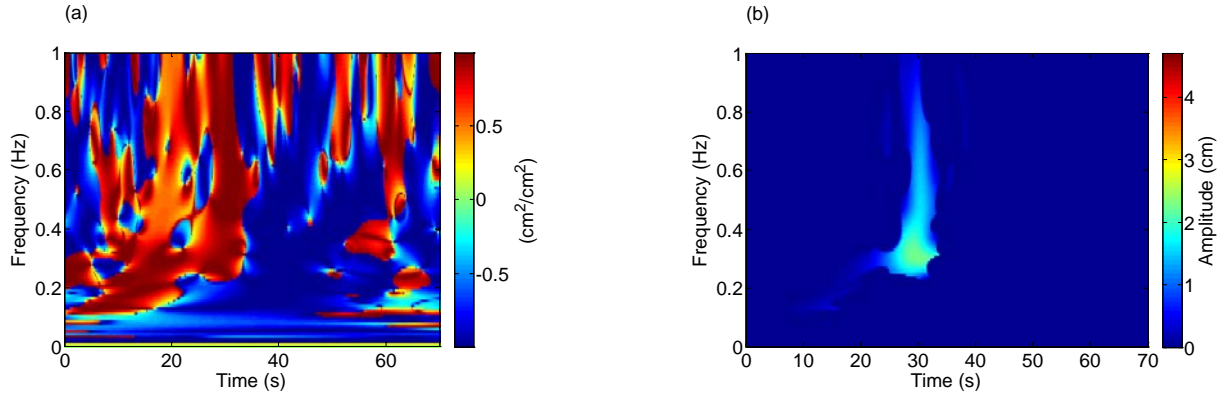


Figure 20. Extraction of pro-grade Rayleigh wave from recording at station TCU116. (a) Normalized inner product of and phase delayed component, (b) Amplitude of component filtered with the NIP criterion.

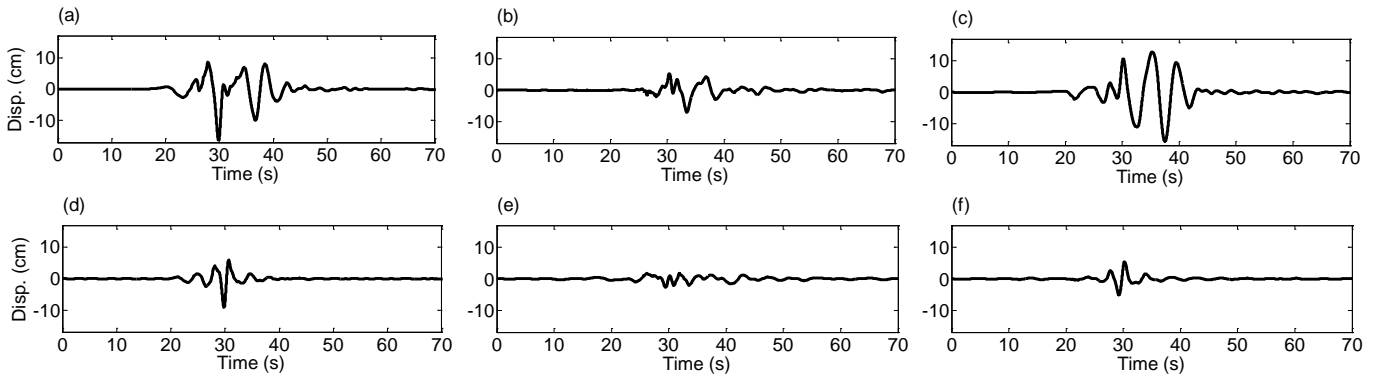


Figure 21. Rayleigh pro-grade wave extracted at station TCU116. (a) Unfiltered radial component, (b) Unfiltered transverse component, (c) Unfiltered vertical component, (d) Extracted radial component, (e) Extracted transverse component, (f) Extracted vertical component.

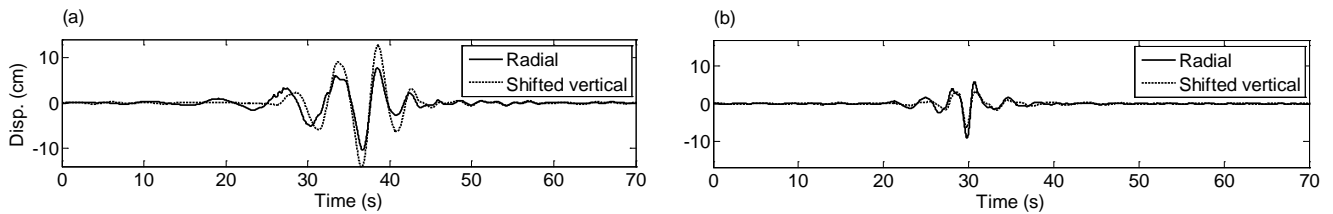


Figure 22. Comparison of radial and shifted vertical components of extracted Rayleigh waves at station TCU116. (a) Retro-grade wave, (b) Pro-grade wave.

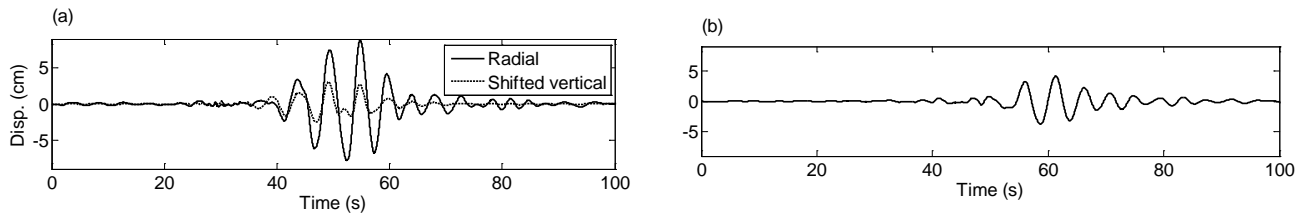


Figure 23. *R-T-V* displacement components of extracted waves at station TCU118. (a) Comparison of radial and shifted vertical component of retro-grade Rayleigh wave (b) Extracted (Love) wave in transverse direction.

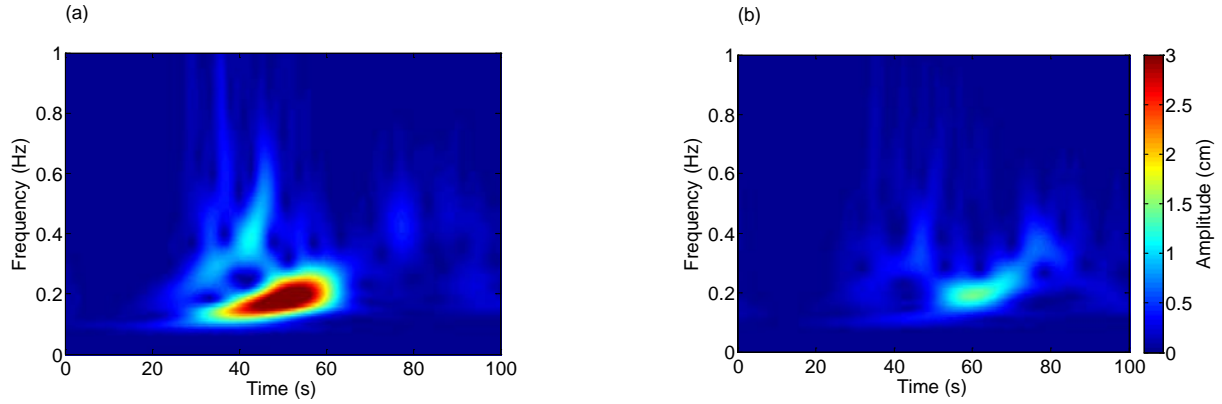


Figure 24. Radial and Transverse time-frequency components for unfiltered recording at station TCU118. (a) Amplitude of radial component (b) Amplitude of transverse component.

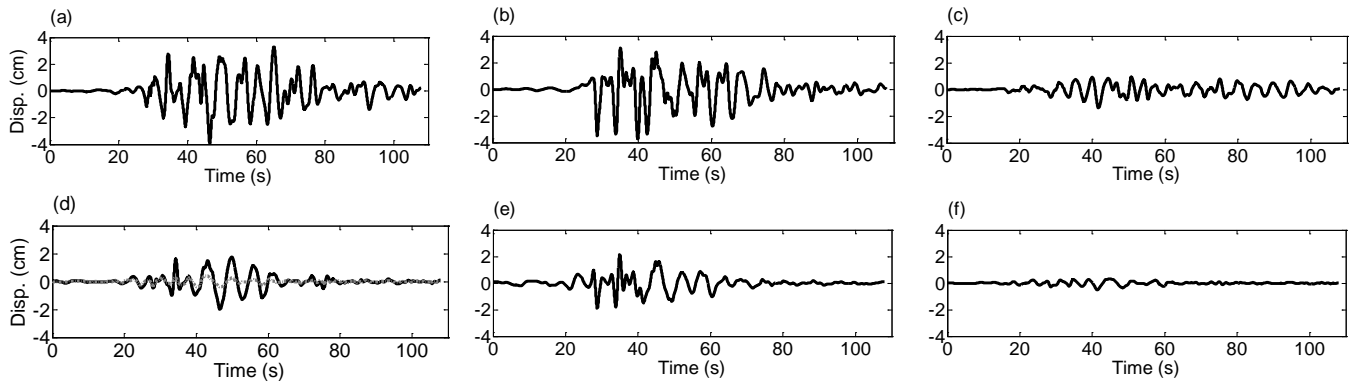


Figure 25. Extracted waves from recording at station CHY107. (a) Unfiltered radial component, (b) Unfiltered transverse component, (c) Unfiltered vertical component, (d) Extracted radial component (black line) and shifted vertical component (gray line), (e) Extracted transverse component, (f) Extracted vertical component.

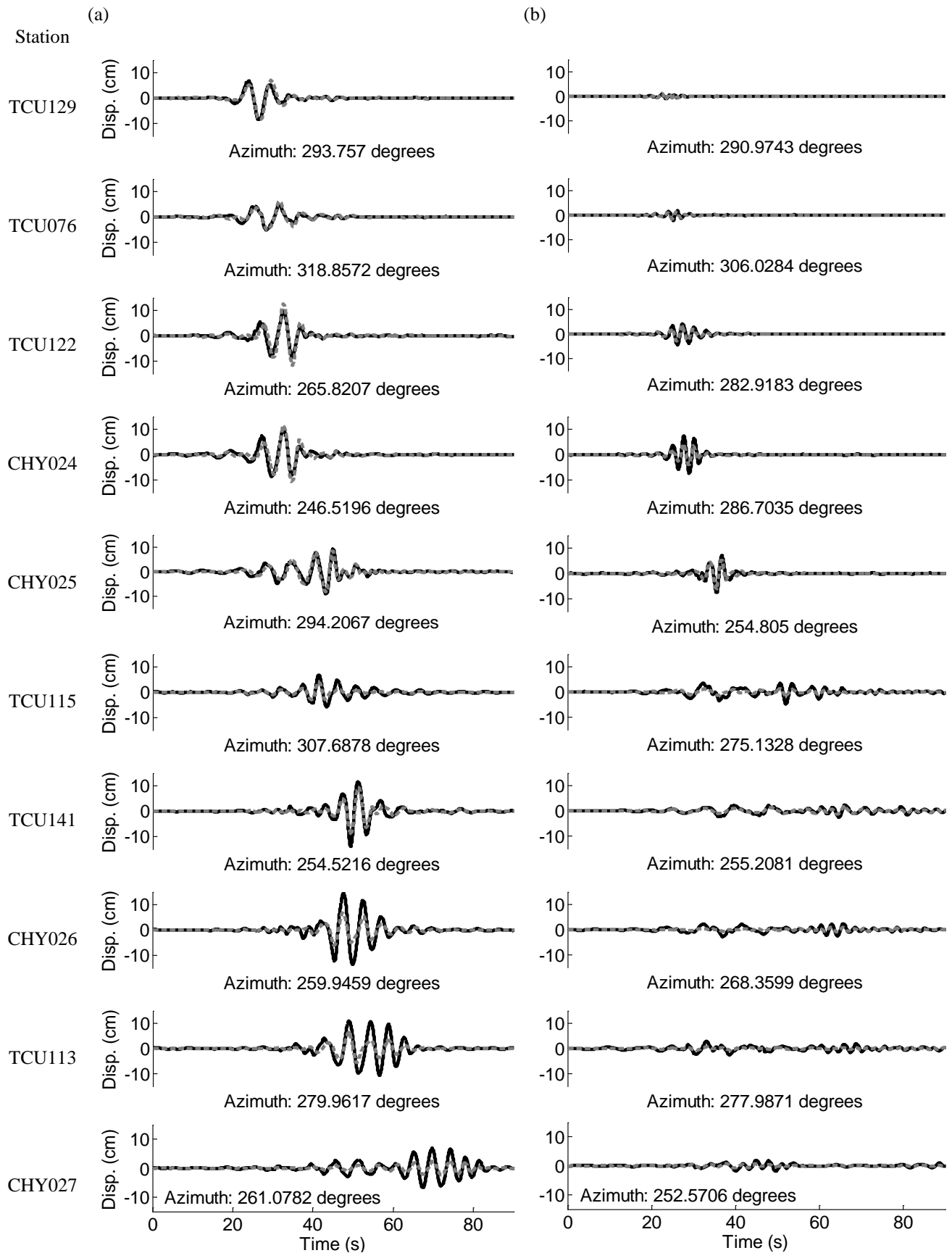


Figure 26. Radial component (black solid line) and shifted vertical component (gray dashed line) of extracted Rayleigh waves at different stations of the WCP plain in Taiwan. (a) Retro-grade waves, (b) Pro-grade waves.

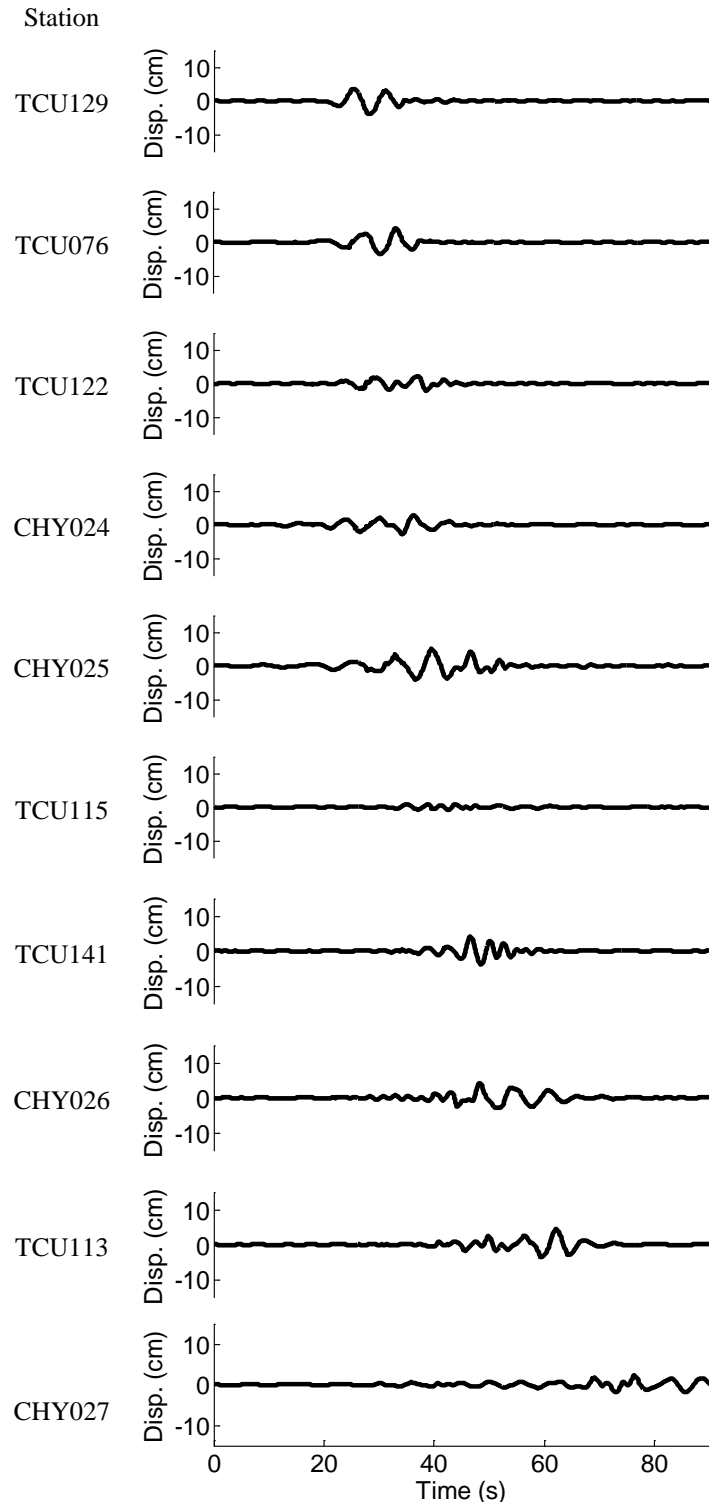


Figure 27. Extracted Love waves at different stations of the WCP plain in Taiwan.